

Numerical simulations of inflationary dynamics: slow-roll and beyond

Siddharth S. Bhatt,^a Swagat S. Mishra,^b Soumen Basak^a and Surya N. Sahoo^c

^aSchool of Physics, Indian Institute of Science Education and Research, Thiruvananthapuram 695551, India.

^bCentre for Astronomy and Particle Theory, School of Physics and Astronomy, University Park Campus, University of Nottingham, Nottingham NG7 2RD, UK.

^cNational Institute of Science Education and Research, Bhubaneswar, Odisha 752050, India.

E-mail: bhattsidharth17@alumni.iisertvm.ac.in,
swagat.mishra@nottingham.ac.uk, sbasak@iisertvm.ac.in, suryans@niser.ac.in

Abstract. Cosmic inflation is a period of rapid accelerated expansion of space in the very early universe. During inflation, vacuum quantum fluctuations are amplified and stretched to cosmological scales which seed the fluctuations in the cosmic microwave background as well as the large-scale structure of our universe. Large quantum fluctuations may lead to the formation of primordial black holes (PBHs) in the post-inflationary universe. Numerical simulations of the inflationary dynamics are presented here for a single canonical scalar field minimally coupled to gravity. We spell out the basic equations governing the inflationary dynamics in terms of cosmic time t and define a set of dimensionless variables convenient for numerical analysis. We then provide a link to our simple numerical `Python` code on `GitHub` that can be used to simulate the background dynamics as well as the evolution of linear perturbations during inflation. The code computes both scalar and tensor power spectra for a given inflaton potential $V(\phi)$. We discuss a concrete algorithm to use the code for various purposes, especially for computing the enhanced scalar power spectrum in the context of PBH formation. We intend to extend the framework to simulate the dynamics of a number of different quantities, including the computation of scalar-induced second-order tensor power spectrum in the revised version of this manuscript in the near future.

Keywords: Inflation, Early Universe Theory, Numerical Analysis

Contents

1	Introduction	1
2	Inflationary Dynamics	3
3	Quantum fluctuations during inflation	6
3.1	Large scale primordial fluctuations	9
3.2	Small-scale primordial fluctuations	12
4	Numerical analysis of inflationary background dynamics	15
4.1	Phase-space analysis	19
4.2	Quantum fluctuations under the slow-roll approximation	20
5	Numerical analysis for quantum fluctuations during inflation	21
5.1	Numerical analysis for slow-roll potentials	24
5.2	Numerical analysis for potentials with a local bump/dip feature	25
6	Future extension of our numerical framework	28
7	Discussion	32
8	Acknowledgements	33

1 Introduction

Cosmic inflation has emerged as the leading scenario for describing the very early universe prior to the commencement of the radiative hot Big Bang Phase [1–6]. According to the inflationary paradigm, a transient epoch of at least 60-70 e-folds of rapid accelerated expansion suffices in setting natural initial conditions for the background space-time in the form of spatial flatness as well as statistical homogeneity and isotropy on large angular scales [2–4, 7]. Additionally, (and more significantly,) quantum fluctuations during inflation naturally generate a spectrum of almost scale-invariant initial scalar fluctuations which seed the temperature and polarisation fluctuations in the Cosmic Microwave Background (CMB) Radiation, and later, the formation of structure in the universe [7–11]. In addition to scalar perturbations, quantum fluctuations during inflation also create a spectrum of almost scale-invariant tensor perturbations which later become gravitational waves [12, 13].

The simplest models of inflation comprising of a single scalar field, called the ‘inflaton’, which is minimally coupled to gravity, makes several distinct predictions [14] (*i.e.* an almost scale-invariant, nearly Gaussian, and adiabatic spectrum of scalar fluctuations) most of which have received spectacular observational confirmation, particularly from the latest CMB missions [15].

However, as mentioned earlier, inflation also generates tensor perturbations that later constitute the relic gravitational wave background (GW) which imprints a distinct signature on the CMB power spectrum in the form of the B-mode polarization [15]. The amplitude of these relic GWs provides us information about the inflationary energy scale while their spectrum enables us to access general properties of the epoch of reheating, being exceedingly

sensitive to the post-inflationary equation of state [13, 16]. The amplitude of inflationary tensor fluctuations, relative to that of scalar fluctuations, is usually characterised by the tensor-to-scalar ratio r . Different models of inflation predict different values for r which is sensitive to the gradient of the inflaton potential $V_{,\phi}(\phi) = \frac{dV(\phi)}{d\phi}$ relative to its height $V(\phi)$. Convex potentials predict large values for r , while concave potentials predict relatively small values of r . While the spectrum of inflationary tensor fluctuations has not yet been observed, current CMB observations are able to place an upper bound on the tensor-to-scalar ratio on large angular scales. In particular, the latest CMB observations of BICEP/Keck [17], combined with those of the PLANCK mission [15], place the strong upper bound $r \leq 0.036$ (at 95% confidence).

This most recent upper bound on r has important consequences for single field canonical inflation. In particular, given $r \leq 0.036$, all monotonically increasing convex potentials, including the whole family of monomial potentials $V(\phi) \propto \phi^p$, are completely ruled out in the canonical framework. Among these strongly disfavoured models are the simplest classic inflaton potentials $\frac{1}{2}m^2\phi^2$ and $\lambda\phi^4$. Instead, the observational upper bound on r appears to favour asymptotically-flat potentials possessing one or two plateau-like wings; see [18, 19]. Current observational data lead to a scenario in which the inflaton ϕ slowly rolls down a shallow potential $V(\phi)$ thereby giving rise to a quasi-de Sitter early stage of near-exponential expansion. A thorough analysis of the inflationary phase-space dynamics $\{\phi, \dot{\phi}\}$ for plateau potentials shows [20] that a large range of initial conditions leads to adequate inflation in these models.

However, it is important to stress that the CMB window constitutes only a tiny part of the observationally available field space between the Hubble-exit of the largest scales in the sky and the smallest scale at the end of inflation. Consequently, a substantial period of the inflationary dynamics corresponding to potentially interesting small-scale primordial physics (which accounts roughly to the last 40–50 e-folds of accelerated expansion during inflation) remains observationally unexplored, being inaccessible to the CMB and LSS observations. Any departure from the slow-roll regime, that might be triggered by a change in the dynamics of the inflaton field, would lead to interesting observational consequences on small-scales. In particular, the presence of a feature at intermediate field values that might lead to large enough amplification of the small-scale scalar fluctuations, would facilitate the formation of Primordial Black Holes upon the Hubble re-entry of these modes during the post-inflationary epochs.

Primordial Black Holes (PBHs) are extremely interesting compact objects which might have been formed from the collapse of large density fluctuations in the early universe [21–24] and they constitute a potential candidate for dark matter [25–30]. Seeds for such large fluctuations can be generated during inflation, as mentioned above. For instance, a feature in the inflaton potential in the form of a flat inflection point can further slow down the already slowly rolling inflaton field substantially, leading to an enhancement of the primordial scalar power P_{ζ} . A number of different features for enhancing small-scale power during inflation have been proposed in the recent years [31–49]. Hence PBHs (and the associated induced relic GWs) are excellent probes of the small-scale primordial physics.

In this preliminary version of our paper, we discuss a simple code developed for numerical simulations of the inflationary dynamics. We introduce the relevant dimensionless variables used in our numerical analysis and provide a link to the code in our [GitHub](#) account. We also discuss how to use the code in various scenarios, which include phase-space analysis of inflationary initial conditions, inflationary background dynamics and determining scalar and

tensor power spectra both under slow-roll approximation and beyond. The latter case has important implications for PBH formation and we discuss how to use the code to simulate the Mukhanov-Sasaki equation mode by mode. We also discuss a number of important future directions that are to be included in the forthcoming version of our paper. The primary version of our numerical framework is quite simple and less compact. It is intended to provide a pedagogical guideline for researchers who are relatively new to numerical simulations of inflation. In the forthcoming version of our work, we will introduce a much more compact numerical framework that we are currently working on which will incorporate additional new features.

This paper is organised as follows: we begin with a brief introduction of the inflationary scalar field dynamics in section 2 and quantum fluctuations in section 3. We then proceed to discuss numerical simulations of the background dynamics in section 4. This also includes studying the scalar and tensor fluctuations under the slow-roll approximations. Section 5 is dedicated to studying the inflationary quantum fluctuations by numerically solving the Mukhanov-Sasaki equation, and its application to inflaton potentials possessing a slow-roll violating feature. We also mention a number of future extensions of our numerical set-up in section 6, before concluding with a discussion section.

We work in the units $c, \hbar = 1$. The reduced Planck mass is defined to be $m_p \equiv 1/\sqrt{8\pi G} = 2.43 \times 10^{18}$ GeV. We assume the background universe to be described by a spatially flat Friedmann-Lemaître-Robertson-Walker (FLRW) metric with signature $(-, +, +, +)$.

2 Inflationary Dynamics

The Action for a scalar field which couples minimally to gravity has the following general form

$$S[\phi] = \int d^4x \sqrt{-g} \mathcal{L}(F, \phi), \quad (2.1)$$

where the Lagrangian density $\mathcal{L}(\phi, F)$ is a function of the field ϕ and the kinetic term

$$F = \frac{1}{2} \partial_\mu \phi \partial^\mu \phi. \quad (2.2)$$

Varying (2.1) with respect to ϕ results in the equation of motion

$$\frac{\partial \mathcal{L}}{\partial \phi} - \left(\frac{1}{\sqrt{-g}} \right) \partial_\mu \left(\sqrt{-g} \frac{\partial \mathcal{L}}{\partial (\partial_\mu \phi)} \right) = 0. \quad (2.3)$$

The energy-momentum tensor associated with the scalar field is

$$T^{\mu\nu} = \left(\frac{\partial \mathcal{L}}{\partial F} \right) (\partial^\mu \phi \partial^\nu \phi) - g^{\mu\nu} \mathcal{L}. \quad (2.4)$$

Specializing to a spatially flat FRW universe and a homogeneous scalar field, one gets

$$ds^2 = -dt^2 + a^2(t) [dx^2 + dy^2 + dz^2], \quad (2.5)$$

$$T^\mu{}_\nu = \text{diag}(-\rho_\phi, p_\phi, p_\phi, p_\phi), \quad (2.6)$$

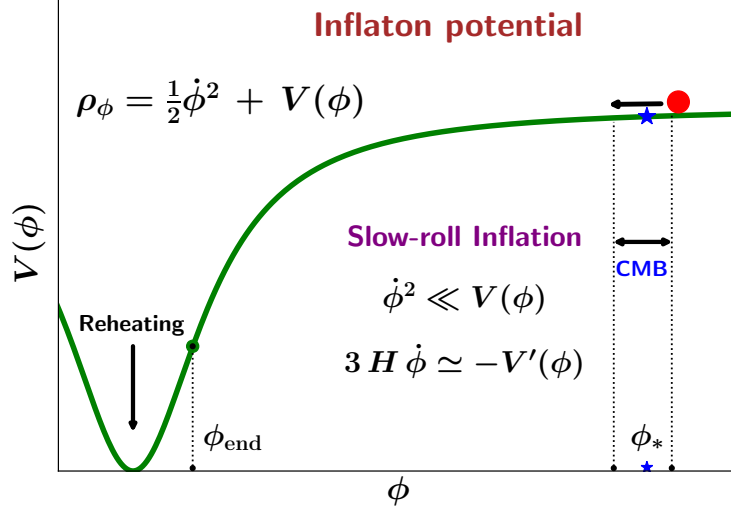


Figure 1: This figure schematically depicts a prototype inflation potential $V(\phi)$, plotted in solid green curve. The ‘CMB Window’ represents field values corresponding to the Hubble-exit epochs of scales $k \in [0.0005, 0.5] \text{ Mpc}^{-1}$ that are observable by the latest CMB missions.

where the energy density, ρ_ϕ , and pressure, p_ϕ , are given by

$$\rho_\phi = \left(\frac{\partial \mathcal{L}}{\partial F} \right) (2F) - \mathcal{L}, \quad (2.7)$$

$$p_\phi = \mathcal{L}, \quad (2.8)$$

and $F = -(\dot{\phi}^2/2)$. The evolution of the scale factor $a(t)$ is governed by the Friedmann equations:

$$\left(\frac{\dot{a}}{a} \right)^2 \equiv H^2 = \frac{1}{3m_p^2} \rho_\phi, \quad (2.9)$$

$$\frac{\ddot{a}}{a} \equiv \dot{H} + H^2 = -\frac{1}{6m_p^2} (\rho_\phi + 3p_\phi), \quad (2.10)$$

where $H \equiv \dot{a}/a$ is the Hubble parameter and ρ_ϕ satisfies the conservation equation

$$\dot{\rho}_\phi = -3H(\rho_\phi + p_\phi). \quad (2.11)$$

In the standard single field inflationary paradigm, inflation is sourced by a minimally coupled canonical scalar field ϕ with a suitable potential $V(\phi)$ (see figure 1). For such a canonical scalar field

$$\mathcal{L}(F, \phi) = -F - V(\phi), \quad (2.12)$$

Substituting (2.12) into (2.7) and (2.8), we find

$$\begin{aligned} \rho_\phi &= \frac{1}{2} \dot{\phi}^2 + V(\phi), \\ p_\phi &= \frac{1}{2} \dot{\phi}^2 - V(\phi), \end{aligned} \quad (2.13)$$

consequently the two Friedmann equations (2.9), (2.10) and the equation (2.11) become

$$H^2 \equiv \frac{1}{3m_p^2} \rho_\phi = \frac{1}{3m_p^2} \left[\frac{1}{2} \dot{\phi}^2 + V(\phi) \right], \quad (2.14)$$

$$\dot{H} \equiv \frac{\ddot{a}}{a} - H^2 = -\frac{1}{2m_p^2} \dot{\phi}^2, \quad (2.15)$$

$$\ddot{\phi} + 3H\dot{\phi} + V_{,\phi}(\phi) = 0. \quad (2.16)$$

The epoch of inflation at any time $t < t_{\text{end}}$ is conveniently marked by the number of e-folds before the end of inflation

$$N_e = \log_e \frac{a_{\text{end}}}{a(t)} = \int_t^{t_{\text{end}}} H(t') dt', \quad (2.17)$$

where $H(t)$ is the Hubble parameter during inflation. $a(t)$ and a_{end} denote the scale factor at time t and at the end of inflation respectively. Typically a period of quasi-de Sitter inflation lasting for at least 60-70 e-folds is required in order to address the problems of the standard hot Big Bang model. We denote N_* as the number of e-folds (before the end of inflation) when the CMB pivot scale $k_* = (aH)_* = 0.05 \text{ Mpc}^{-1}$ left the comoving Hubble radius during inflation. For convenience, we have chosen $N_* = 60$ for the most part of this work, although the exact value of N_* depends upon the particular detail of reheating history.

The quasi-de Sitter like phase corresponds to the inflaton field rolling slowly down the potential $V(\phi)$. This slow-roll regime¹ of inflation, ensured by the presence of the Hubble friction term in the equation (2.16), is usually characterised by the first two kinematical Hubble slow-roll parameters ϵ_H , η_H , defined by [7]

$$\epsilon_H = -\frac{\dot{H}}{H^2} = \frac{1}{2m_p^2} \frac{\dot{\phi}^2}{H^2}, \quad (2.18)$$

$$\eta_H = -\frac{\ddot{\phi}}{H\dot{\phi}} = \epsilon_H + \frac{1}{2\epsilon_H} \frac{d\epsilon_H}{dN_e}, \quad (2.19)$$

where the slow-roll regime of inflation corresponds to

$$\epsilon_H, \eta_H \ll 1. \quad (2.20)$$

The slow-roll regime is also often characterised by the dynamical potential slow-roll parameters [7], defined by

$$\epsilon_V = \frac{m_p^2}{2} \left(\frac{V_{,\phi}}{V} \right)^2, \quad \eta_V = m_p^2 \left(\frac{V_{,\phi\phi}}{V} \right). \quad (2.21)$$

For small values of these parameters $\epsilon_H, \eta_H \ll 1$, one finds $\epsilon_H \simeq \epsilon_V$ and $\eta_H \simeq \eta_V - \epsilon_V$. Using the definition of Hubble parameter, $H = \dot{a}/a$, we have $\ddot{a}/a = \dot{H} + H^2 = H^2(1 + \dot{H}/H^2)$. From the expression for ϵ_H in (2.18), it is easy to see that

$$\frac{\ddot{a}}{a} = (1 - \epsilon_H) H^2. \quad (2.22)$$

Which implies that the universe accelerates, $\ddot{a} > 0$, when $\epsilon_H < 1$. Using equation (2.14), the expression for ϵ_H in (2.18) reduces to $\epsilon_H \simeq \frac{3}{2} \frac{\dot{\phi}^2}{V}$ when $\dot{\phi}^2 \ll V$.

¹It is well known that the slow-roll phase of the inflation is actually a local attractor for many different models of inflation, see [20, 50] and the references therein.

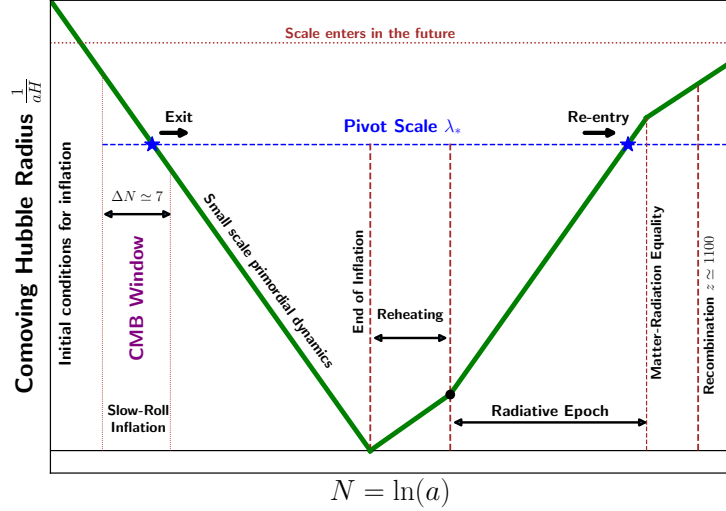


Figure 2: This figure schematically illustrates the evolution of the comoving Hubble radius $(aH)^{-1}$ with scale factor. During inflation $(aH)^{-1}$ decreases which causes physical scales to exit the Hubble radius. After inflation ends $(aH)^{-1}$ increases, and physical scales begin to re-enter the Hubble radius. The CMB pivot scale, as used by the Planck mission, is set at $k_* = 0.05 \text{ Mpc}^{-1}$ and has been depicted by the dashed blue line. The ‘CMB Window’ corresponds to the scales $k \in [0.0005, 0.5] \text{ Mpc}^{-1}$ that are observable by the latest CMB missions. Note that $(aH)^{-1} \propto a$ during the radiative regime and $(aH)^{-1} \propto a^{-1}$ during inflation.

3 Quantum fluctuations during inflation

In the standard scenario of a minimally coupled single canonical scalar field ϕ as the inflaton, two gauge-independent massless fields, one scalar, and one transverse traceless tensor, get excited during inflation and receive quantum fluctuations that are correlated over super-Hubble scales [51] at late times.

Scalar fluctuations

The evolution of the scalar degree of freedom, called the curvature perturbation² ζ is described by the following quadratic Action [7, 52]

$$S_{(2)}[\zeta] = \frac{1}{2} \int d\tau dx^3 z^2 [(\zeta')^2 - (\partial_i \zeta)^2], \quad (3.1)$$

which upon the change of variable

$$v \equiv z \zeta, \quad \text{with} \quad z = a m_p \sqrt{2\epsilon_H} = a \frac{\dot{\phi}}{H}, \quad (3.2)$$

²Note that the comoving curvature perturbation \mathcal{R} is related to the curvature perturbation on uniform-density hypersurfaces, ζ , and both are equal during slow-roll inflation as well as on super-Hubble scales, $k \ll aH$, in general (see [7]).

takes the form

$$S_{(2)}[v] = \frac{1}{2} \int d\tau dx^3 \left[(v')^2 - (\partial_i v)^2 + \frac{z''}{z} v^2 \right], \quad (3.3)$$

where the $(')$ denotes derivative with respect to conformal time $\tau = \int \frac{dt}{a(t)}$ ($\simeq \frac{-1}{aH}$ for quasi-de Sitter expansion). The variable v , which itself is a scalar quantum field like ζ , is called the *Mukhanov-Sasaki variable* in literature. Its Fourier modes v_k satisfy the famous Mukhanov-Sasaki equation given by [53, 54]

$$\boxed{v_k'' + \left(k^2 - \frac{z''}{z} \right) v_k = 0}, \quad (3.4)$$

where the effective mass term is given by the following exact expression [55]

$$\boxed{\frac{z''}{z} = (aH)^2 \left(2 - \epsilon_1 + \frac{3}{2}\epsilon_2 + \frac{1}{4}\epsilon_2^2 - \frac{1}{2}\epsilon_1\epsilon_2 + \frac{1}{2}\epsilon_2\epsilon_3 \right)}, \quad (3.5)$$

$$\Rightarrow \boxed{\frac{z''}{z} = (aH)^2 \left[2 + 2\epsilon_H - 3\eta_H + 2\epsilon_H^2 + \eta_H^2 - 3\epsilon_H\eta_H - \frac{1}{aH} \eta_H' \right]}, \quad (3.6)$$

with $\epsilon_1 = \epsilon_H$ and where

$$\epsilon_{n+1} = -\frac{d \ln \epsilon_n}{dN_e} \quad (3.7)$$

are the ‘Hubble flow’ parameters. Given a mode k , at sufficiently early times when it is sub-Hubble i.e $k \gg aH$, we can assume v to be in the Bunch-Davies vacuum [56] satisfying

$$v_k \rightarrow \frac{1}{\sqrt{2k}} e^{-ik\tau}. \quad (3.8)$$

During inflation as the comoving Hubble radius falls (see figure 2), modes start becoming super-Hubble i.e $k \ll aH$ and equation (3.4) dictates that $|v_k| \propto z$ and hence ζ_k approaches a constant value. By solving the Mukhanov-Sasaki equation we can estimate the dimensionless primordial power spectrum of ζ using the following relation [51]

$$\boxed{P_\zeta \equiv \frac{k^3}{2\pi^2} |\zeta_k|^2 \Big|_{k \ll aH} = \frac{k^3}{2\pi^2} \frac{|v_k|^2}{z^2} \Big|_{k \ll aH}}. \quad (3.9)$$

During slow-roll inflation, the factor $\frac{z''}{z} = \frac{\nu^2 - 0.25}{\tau^2}$ with $\nu \approx 1.5 + \epsilon_H + \frac{\dot{\epsilon}_H}{2H\epsilon_H}$. Solving the Mukhanov-Sasaki equation with suitable Bunch-Davies vacuum conditions leads to the famous slow-roll approximation formula [7]

$$\boxed{P_\zeta = \frac{1}{8\pi^2} \left(\frac{H}{m_p} \right)^2 \frac{1}{\epsilon_H}}. \quad (3.10)$$

Note that one could also directly try to solve for the fourier modes of the comoving curvature perturbation ζ (instead of the Mukhanov-Sasaki variable v) which satisfies the equation

$$\boxed{\zeta_k'' + 2 \left(\frac{z'}{z} \right) \zeta_k' + k^2 \zeta_k = 0} \quad (3.11)$$

and implement the corresponding Bunch-Davies initial conditions for ζ_k . The friction term in equation (3.11) is given by

$$\boxed{\frac{z'}{z} = aH (1 + \epsilon_H - \eta_H)} . \quad (3.12)$$

Before moving forward, we stress that the slow-roll regime of inflation necessarily requires both the slow-roll parameters to be small *i.e* $\epsilon_H \ll 1$ and $\eta_H \ll 1$. Violation of either of these conditions invalidates the above analytical treatment. When either of the slow-roll conditions is violated, which is the situation in the context of primordial black hole formation, a more accurate determination of P_ζ is provided by solving the Mukhanov-Sasaki equation (3.4) numerically. The computation of power spectrum when the slow-roll approximation is violated will be our primary focus.

Tensor fluctuations

The corresponding quadratic Action for tensor fluctuations is given by [7, 52]

$$\boxed{S_{(2)}[\gamma_{ij}] = \frac{1}{2} \int d\tau d^3x a^2 \left(\frac{m_p}{2} \right)^2 [(\gamma'_{ij})^2 - (\partial \gamma_{ij})^2]} . \quad (3.13)$$

The Mukhanov-Sasaki variable for tensor fluctuations are defined as

$$\frac{m_p}{2} a \gamma_{ij} \equiv \begin{pmatrix} h_+ & h_\times & 0 \\ h_\times & -h_+ & 0 \\ 0 & 0 & 0 \end{pmatrix} \quad (3.14)$$

or,

$$\frac{m_p}{2} a \gamma_{ij} \equiv \sum_{s=+,\times} \Pi_{ij}^s h_s , \quad (3.15)$$

where Π^+ and Π^\times are the 2 polarization modes, written as

$$\Pi_{ij}^+ = \begin{pmatrix} 1 & 0 & 0 \\ 0 & -1 & 0 \\ 0 & 0 & 0 \end{pmatrix} \quad \text{and} \quad \Pi_{ij}^\times = \begin{pmatrix} 0 & 1 & 0 \\ 1 & 0 & 0 \\ 0 & 0 & 0 \end{pmatrix} . \quad (3.16)$$

Thus,

$$\gamma_{ij} = \frac{2}{m_p} \sum_{s=+,\times} \Pi_{ij}^s \frac{h_s}{a} . \quad (3.17)$$

The evolution equation for the mode functions (by dropping the ‘s’ subscript and remembering that it is summed over for 2 polarization states) is given by

$$\boxed{h_k'' + \left(k^2 - \frac{a''}{a} \right) h_k = 0} . \quad (3.18)$$

The subsequent computation of tensor power spectrum

$$P_T(k) \equiv 2 \times \frac{k^3}{2\pi^2} \frac{|h_k|^2}{a^2} \Big|_{k \ll aH} , \quad (3.19)$$

under quasi-de Sitter approximation leads to [7]

$$P_T(k) = \frac{2}{\pi^2} \left(\frac{H}{m_p} \right)^2. \quad (3.20)$$

Note that, unlike the Mukhanov-Sasaki equation (3.4) for scalar fluctuations, the tensor mode equation (3.18) does not depend upon z , rather it depends only upon the scale factor a . Hence, as long as the quasi-de Sitter approximation is valid, *i.e.* $\epsilon_H \ll 1$, power spectrum of tensor fluctuations does not get affected by an appreciable amount even if slow-roll is violated. Although, this statement is true only at linear order in perturbation theory. Tensor fluctuations at second order in perturbation theory can be induced by large first-order scalar fluctuations [57–60] (also see [61] and references therein).

3.1 Large scale primordial fluctuations

On large cosmological scales which are accessible to CMB observations, the scalar power spectrum typically takes the form of a power law represented by

$$P_\zeta(k) = A_S \left(\frac{k}{k_*} \right)^{n_S - 1}, \quad (3.21)$$

where $A_S = P_\zeta(k_*)$ is the amplitude of the scalar power spectrum at the pivot scale $k = k_*$, given by³

$$A_S = \frac{1}{8\pi^2} \left(\frac{H}{m_p} \right)^2 \frac{1}{\epsilon_H} \Big|_{\phi=\phi_*}, \quad (3.22)$$

where ϕ_* is the value of the inflaton field at the epoch of Hubble exit of the CMB pivot scale k_* . The scalar spectral tilt n_S , in the slow-roll regime is given by [7]

$$n_S - 1 \equiv \frac{d \ln P_\zeta}{d \ln k} = 2\eta_H - 4\epsilon_H. \quad (3.23)$$

Similarly the tensor power spectrum, in the slow-roll limit, is represented by

$$P_T(k) = A_T \left(\frac{k}{k_*} \right)^{n_T}, \quad (3.24)$$

with the amplitude of tensor power spectrum at the CMB pivot scale is given by [7, 51]

$$A_T \equiv P_T(k_*) = \frac{2}{\pi^2} \left(\frac{H}{m_p} \right)^2 \Big|_{\phi=\phi_*}, \quad (3.25)$$

and the tensor spectral index (with negligible running) is given by

$$n_T = -2\epsilon_H. \quad (3.26)$$

³Note that in general, k may correspond to any observable CMB scale in the range $k \in [0.0005, 0.5] \text{ Mpc}^{-1}$. However, in order to derive constraints on the inflationary observables $\{n_S, r\}$, we mainly focus on the CMB pivot scale, namely $k \equiv k_* = 0.05 \text{ Mpc}^{-1}$.

The tensor-to-scalar ratio r is defined by

$$r \equiv \frac{A_T}{A_S} = 16 \epsilon_H , \quad (3.27)$$

yielding the single field consistency relation

$$r = -8 n_T . \quad (3.28)$$

Hence the slow-roll parameters ϵ_H and η_H play an important role in characterising the power spectra of scalar and tensor fluctuations during inflation. Before going forward, we briefly discuss the implications of the latest CMB observations for the slow-roll parameters as well as for other relevant inflationary observables. In order to relate the CMB observables to the inflaton potential $V(\phi)$, we work with the potential slow-roll parameters defined in equation (2.21).

Consider a canonical scalar field minimally coupled to gravity and having the potential

$$V(\phi) = V_0 f \left(\frac{\phi}{m_p} \right) . \quad (3.29)$$

The potential slow-roll parameters (2.21) are given by

$$\epsilon_V = \frac{m_p^2}{2} \left(\frac{f, \phi}{f} \right)^2 , \quad (3.30)$$

$$\eta_V = m_p^2 \left(\frac{f, \phi \phi}{f} \right) . \quad (3.31)$$

In the slow-roll limit $\epsilon_V, \eta_V \ll 1$, the scalar power spectrum is given by the expression (3.21) with the amplitude of scalar power at the CMB pivot scale $k \equiv k_* = 0.05 \text{ Mpc}^{-1}$ expressed as [7]

$$A_S \equiv P_\zeta(k_*) \simeq \frac{1}{24\pi^2} \frac{V_0}{m_p^4} \frac{f(\phi_k)}{\epsilon_V(\phi_k)} \Big|_{k=k_*} , \quad (3.32)$$

and the scalar spectral index (with negligible running) is given by

$$n_S \simeq 1 + 2 \eta_V(\phi_*) - 6 \epsilon_V(\phi_*) , \quad (3.33)$$

Similarly the amplitude of tensor power spectrum at the CMB pivot scale is given by

$$A_T \equiv P_T(k_*) = \frac{2}{\pi^2} \left(\frac{H}{m_p} \right)^2 \Big|_{\phi=\phi_*} \simeq \frac{2}{3\pi^2} \frac{V_0}{m_p^4} f(\phi_*) , \quad (3.34)$$

and the tensor spectral index (3.26) becomes

$$n_T \simeq -2 \epsilon_V(\phi_*) , \quad (3.35)$$

and the tensor-to-scalar ratio (3.27) can be written as

$$r \simeq 16 \epsilon_V(\phi_*) , \quad (3.36)$$

satisfying the single field consistency relation (3.28). From the CMB observations of Planck 2018 [15], we have

$$A_s = 2.1 \times 10^{-9} , \quad (3.37)$$

while the 2σ constraint on the scalar spectral index is given by

$$n_s \in [0.957, 0.976] . \quad (3.38)$$

Similarly the constraint on the tensor-to-scalar ratio r , from the latest combined observations of Planck 2018 [15] and BICEP/Keck [17], is given by

$$r \leq 0.036 , \quad (3.39)$$

which translates into $A_T \leq 3.6 \times 10^{-2} A_s$. Equation (3.34) helps place the following upper bound on the inflationary Hubble scale H^{inf} and the energy scale during inflation E_{inf}

$$H^{\text{inf}} \leq 4.7 \times 10^{13} \text{ GeV} , \quad (3.40)$$

$$E_{\text{inf}} \equiv \left[\sqrt{3} m_p H^{\text{inf}} \right]^{1/2} \leq 1.4 \times 10^{16} \text{ GeV} . \quad (3.41)$$

Similarly the CMB bound on r when combined with (3.36) translates into an upper bound on the first slow-roll parameter

$$\epsilon_H \simeq \epsilon_V \leq 0.00225 , \quad (3.42)$$

rendering the tensor tilt from equation (3.35) to be negligibly small

$$|n_T| \leq 0.0045 . \quad (3.43)$$

Given the upper limit on ϵ_V , using the CMB bound on n_s from (3.38) in (3.33), we infer that the *second slow-roll parameter is negative* and obtain interesting upper and lower limits on its magnitude, given by

$$|\eta_H| \in [0.0075, 0.0215] . \quad (3.44)$$

The EOS w_ϕ of the inflaton field is given by

$$w_\phi = \frac{\frac{1}{2}\dot{\phi}^2 - V(\phi)}{\frac{1}{2}\dot{\phi}^2 + V(\phi)} \simeq -1 + \frac{2}{3}\epsilon_V(\phi) , \quad (3.45)$$

Therefore one finds from (3.42) the following constraint on the inflationary EOS at the pivot scale

$$w_\phi \leq -0.9985 , \quad (3.46)$$

implying that the expansion of the universe during inflation was near exponential (quasi-de Sitter like).

The CMB observations, in the context of single field slow-roll inflationary paradigm, favours asymptotically-flat potentials (featuring either one or two plateau wings) with $n_s \simeq 0.965$ and $r \leq 0.036$. A typical plateau-potential is demonstrated in figure 1 and this is the standard/vanilla scenario. Given that power spectrum is almost scale-invariant with slightly red tilt, *i.e* $n_s - 1 \lesssim 0$, large-scale fluctuations are more important while nothing drastic is expected to happen on smaller cosmological scales that are super-Hubble at the end of inflation.

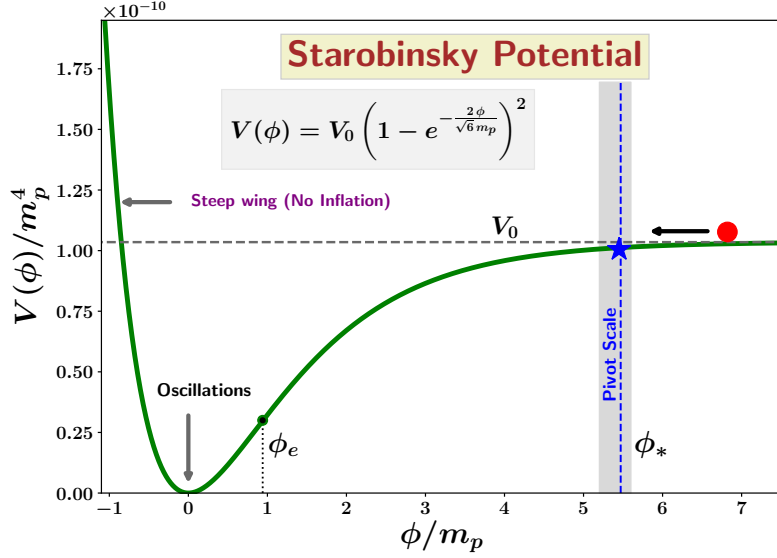


Figure 3: This figure shows the Starobinsky potential (3.48) with CMB pivot scale $k_* = 0.05 \text{ Mpc}^{-1}$ by a blue color star as well as the CMB window $k_{\text{CMB}} \in [0.0005, 0.5] \text{ Mpc}^{-1}$ in grey color shade in the field space. From this figure, it is clear that CMB window constitutes only a tiny portion of the available field space in between ϕ_{CMB} and end of inflation ϕ_e .

Before proceeding further to discuss small-scale inflationary fluctuations, let us make our nomenclature concrete (which is consistent with the standard nomenclature in the inflationary literature).

- **Quasi-de Sitter** inflation corresponds to the condition $\epsilon_H \ll 1$.
- **Slow-roll** inflation corresponds to $\epsilon_H, \eta_H \ll 1$.

This distinction will be important for the rest of the discussions in this paper. Under either of the aforementioned assumptions, the expression for conformal time is given by

$$-\tau \simeq \frac{1}{aH}. \quad (3.47)$$

3.2 Small-scale primordial fluctuations

As mentioned above, the recent CMB observations support the scenario of the inflaton field rolling slowly down an asymptotically-flat potential at the time when the observable CMB scales made their Hubble exit during inflation. However, the current CMB and LSS observations probe only about 7-8 e-folds of inflation around the Hubble exit time of the CMB pivot scale. We explicitly mention that CMB observations probe primordial fluctuations with comoving scales $k_{\text{CMB}} \in [0.0005, 0.5] \text{ Mpc}^{-1}$ (which includes pivot scale $k_* = 0.05 \text{ Mpc}^{-1}$) corresponding to multipole $l \in [2, 2500]$ in the angular sky. Additionally, Lyman- α forest observations enforce constraints on the primordial power spectrum upto $k \simeq \mathcal{O}(1) \text{ Mpc}^{-1}$ (see [29]).

Hence a large portion of evolution during the inflationary phase that accounts roughly to about 50 e-folds of expansion, corresponding to scales smaller than those probed by CMB, remains observationally inaccessible at present. Consequently the associated dynamics of the inflaton field also remains unprobed. For example, figure 3 demonstrates that the CMB window constitutes only a tiny part of the observationally available field space between the largest scales in the sky and the smallest scale at the end of inflation for Starobinsky potential [1, 62]

$$V(\phi) = V_0 \left(1 - e^{-\frac{2}{\sqrt{6}} \frac{\phi}{m_p}} \right)^2. \quad (3.48)$$

Any deviation from the quasi-de Sitter expansion and/or departure from the slow-roll regime $\epsilon_H, \eta_H \ll 1$ that might be triggered by a change in the dynamics of the inflaton field, would lead to interesting observational consequences on small scales. In particular if the inflaton potential possesses a near inflection point-like broad feature at some intermediate field values, then the scalar quantum fluctuations corresponding to scales becoming super-Hubble around the time when the inflaton rolls past such features, might receive enough amplification to facilitate the formation of Primordial Black Holes (PBHs) upon their Hubble re-entry during the radiative epoch.

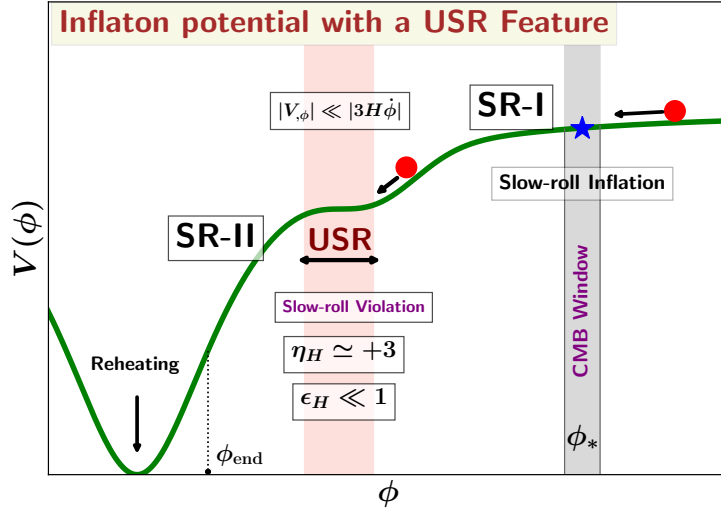


Figure 4: This figure schematically depicts a prototype plateau potential, plotted in solid green curve. The ‘CMB Window’ represents field values corresponding to the Hubble-exit epochs of scales $k \in [0.0005, 0.5] \text{ Mpc}^{-1}$ that are observable by the latest CMB missions. The potential exhibits a small-scale feature (shown in the salmon colour shading) in the form of a flat inflection point-like segment which results in ultra slow-roll (USR) inflation. After exiting the first slow-roll phase (SR-I) near the CMB window, the inflaton enters into an USR phase, during which the second slow-roll condition is violated, namely $\eta_H \simeq +3$. This leads to an enhancement of power spectrum at small-scales. Later, the inflaton emerges out of the USR to another slow-roll phase (SR-II) before the end of inflation.

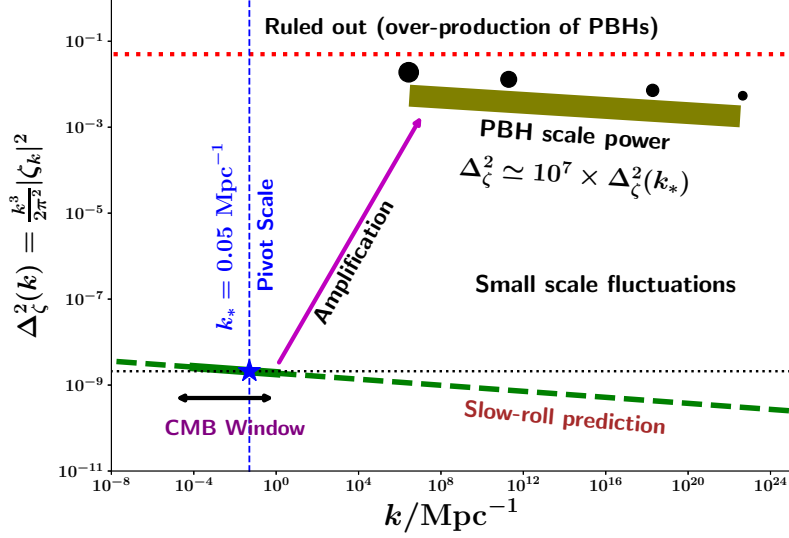


Figure 5: This figure schematically illustrates the typical amplification of inflationary primordial power spectrum at smaller length scales required for PBH formation.

We note that, there are a plethora of possible features that would lead to deviation from standard scale-invariant power spectrum [63]. However, in this paper we will only focus on potentials with a tiny local bump/dip like feature [44] in order to illustrate the efficiency of our numerical analysis. Our code can be used to simulate a number of different types of features in the inflaton potential.

PBH formation requires the enhancement of the inflationary power spectrum by roughly a factor of 10^7 within less than 40 e-folds of expansion (on scales smaller than the pivot scale k_*) as illustrated in figure 5. Therefore the quantity $\Delta \ln \epsilon_H / \Delta N$, and hence also $|\eta_H|$, can grow to become of order unity, thereby violating the second slow-roll condition [64]. In fact the second Hubble slow-roll parameter $|\eta_H|$ becomes larger than unity even though ϵ_H itself remains much smaller than unity. As a result, equation (3.22) can no longer be trusted to compute the power spectrum and one must determine $P_{\mathcal{R}}$ by numerically integrating the Mukhanov-Sasaki equation (3.4).

We proceed as follows. We first discuss the simulations of inflationary background dynamics in section 4, where we also discuss how to generate phase-space portrait $\{\phi, \dot{\phi}\}$ during inflation. In section 5.1, we introduce our numerical scheme for studying quantum fluctuations during slow-roll inflation. We work with convex as well as asymptotically-flat potentials. In section 5.2, we apply our numerical scheme to potentials featuring a local bump/dip like feature that facilitates the amplification of scalar power on small primordial scales. We demonstrate that slow-roll formula (3.22) underestimates both the location as well as the height of scalar power spectrum $\mathcal{P}_\zeta(k)$ for both type of aforementioned features and hence one must solve the Mukhanov-Sasaki equation (3.4) numerically to estimate the power spectrum accurately. We also demonstrate that the growth of the power spectrum obeys the steepest growth bounds discussed in [65–68].

4 Numerical analysis of inflationary background dynamics

A complete analysis of the inflationary background dynamics can be obtained from the evolution of ϕ , $\dot{\phi}$ and H . All of these quantities can be simulated by numerically solving equations (2.14), (2.15) and (2.16). The evolution of the scale factor follows directly from $H = \dot{a}/a$. Our system is defined by the following set of equations (as a function of cosmic time t)

$$H^2 = \frac{1}{3m_p^2} \left[\frac{1}{2} \dot{\phi}^2 + V(\phi) \right], \quad (4.1)$$

$$\dot{H} = -\frac{\dot{\phi}^2}{2m_p}, \quad (4.2)$$

$$\ddot{\phi} = -3H\dot{\phi} - V_{,\phi}(\phi), \quad (4.3)$$

where the functional form of the potential $V(\phi)$ is given by the specific inflationary model. However, the rest of the algorithm is largely model-independent. We can re-write the potential as

$$V(\phi) = V_0 f(\phi). \quad (4.4)$$

In order to carry out numerical simulations, it is convenient to write down the dynamical equations in terms of dimensionless variables (which also ensures that we do not need to worry about keeping track of units). Furthermore, it is important to re-scale the time variable by a factor S which can be suitably chosen according to the energy scale of the dynamics⁴. Our primary dimensionless variables are defined as

$$T = (t m_p) S, \quad (4.5)$$

$$x = \frac{\phi}{m_p}, \quad (4.6)$$

$$y = \left(\frac{\dot{\phi}}{m_p^2} \right) \frac{1}{S}, \quad (4.7)$$

$$z = \left(\frac{H}{m_p} \right) \frac{1}{S}, \quad (4.8)$$

$$A = (a m_p) S. \quad (4.9)$$

In terms of these variables, the dynamical equations (to be simulated) take the form

$$\frac{dx}{dT} = y, \quad (4.10)$$

$$\frac{dy}{dT} = -3zy - \frac{v_0}{S^2} f_{,x}(x), \quad (4.11)$$

$$\frac{dz}{dT} = -\frac{1}{2}y^2, \quad (4.12)$$

$$\frac{dA}{dT} = Az. \quad (4.13)$$

⁴Depending upon the potential, we usually choose the value of S to be in the range $S \in [10^{-5}, 10^{-3}]$.

We can also define the dimensionless potential to be

$$\frac{V(\phi)}{m_p^4} \equiv v_0 f(x) = \frac{V_0}{m_p^4} f(x). \quad (4.14)$$

We can solve the aforementioned set of equations with appropriate initial conditions. In our analysis, we use the `odeint` function provided in the `scipy.integrations` package. By incorporating initial conditions $\{x_i, y_i, z_i, A_i\}$ for the primary dynamical variables $\{x, y, z, A\}$, we simulate their time evolution during inflation. Accordingly, we determine the crucial derived/secondary (dimensionless) dynamical variables from the primary ones by⁵

$$N = \log \frac{A}{A_i} \quad (4.15)$$

$$\epsilon_H = \frac{1}{2} \frac{y^2}{z^2}, \quad \eta_H = -\frac{1}{yz} \frac{dy}{dT}, \quad (4.16)$$

$$A_S = \frac{1}{8\pi^2} \frac{(Sz)^2}{\epsilon_H}, \quad A_T = \frac{2}{\pi^2} (Sz)^2, \quad (4.17)$$

$$n_S = 1 + 2\eta_H - 4\epsilon_H, \quad n_T = -2\epsilon_H, \quad (4.18)$$

$$r = 16\epsilon_H. \quad (4.19)$$

We define N_T to be the number of e-folds of accelerated expansion realised in between an arbitrary initial time and the end of inflation, which is marked by $\epsilon_H = 1$. We then define the more important quantity $N_e = N_T - N$ as the number of e-folds before the end of inflation. Note that $N_e = 0$ at the end of inflation while $N_e > 0$ at early times. This will be our primary time variable against which we will be plotting the dynamics of different inflationary observables. In order to realise adequate amount of inflation, *i.e.* $N_T > 60$, initial value of scalar field must be large enough (and is model dependent). For most large field potentials, this value is of the order $\phi_i \lesssim \mathcal{O}(10) m_p$.

Composing the code involves typing down the dimensionless equations in the appropriate syntax and solving them by using an ODE solver. See our supplementary [Python code](#)⁶ for details. For a particular model of interest, we need to input the inflaton potential in the form $\frac{V(\phi)}{m_p^4} = v_0 f(x)$. Since the slow-roll parameters and the duration N_T do not strongly depend on v_0 , we can initially set its value to roughly $v_0 = 10^{-10}$. We can later adjust the value of v_0 to yield the correct CMB normalised value of scalar power spectrum (3.37) at the pivot scale $N = N_*$. One can proceed in the following step-by-step algorithm.

1. After setting the parameters of the potential and defining the function $f(x)$, we need to incorporate initial conditions for the four primary variables $\{x, y, z, A\}$. We enter appropriate initial conditions x_i, y_i and A_i in the following way. A_i can be set arbitrarily in a spatially flat universe, however depending upon the energy scale of inflation, one can provide an appropriate value. We suggest a typical $A_i = 1 \times 10^{-3}$, although its precise value does not affect the dynamics. In regard to the initial value of x , we need

⁵Note that the observables A_S, A_T, n_S, n_T , and r are related to inflationary scalar and tensor fluctuations and the expressions given here are under slow-roll approximations, *i.e.* $\epsilon_H, |\eta_H| \ll 1$, during which they can be determined purely from the dynamics of background quantities such as H, ϵ_H, η_H . Computation of inflationary power spectra when slow-roll is violated is described in section 5.2.

⁶<https://github.com/bhattsidharth/NumDynInflation>

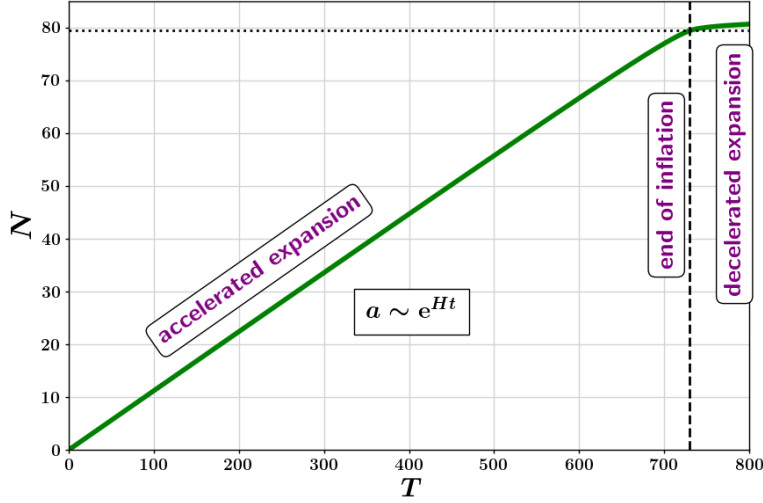


Figure 6: Time evolution of the number of e-folds (scale factor in the logarithm scale) of expansion of the universe is shown for Starobinsky potential (3.48). For the most part of inflation, the expansion is almost exponential (quasi-de Sitter) *i.e* $a \sim e^{Ht}$, leading to a rapid growth in the number of e-folds within a small amount of time. While after the end of inflation, the expansion is decelerated, leading to a much slower growth in the scale factor.

to ensure that x_i is large enough (or small enough if we are working with symmetry breaking hilltop type potentials) to yield adequate amount of inflation, *i.e* $N_T \geq 70$. As mentioned before, the typical value for large field models is $x_i \lesssim \mathcal{O}(10)$.

Since we will be mostly working with potentials that exhibit slow-roll behaviour at initial times, and given that slow-roll trajectory is an attractor in relatively large field models [20], we can safely set $y_i = 0$, as long as x_i is large enough. One can also incorporate slow-roll initial conditions from the beginning, namely $y_i = -\frac{v_0}{3} \frac{f_{,x}}{S_z}$, as is usually done in practice⁷. Finally, the initial value of z can be incorporated in terms of x_i, y_i using the dimensionless Friedmann equation

$$z_i = \sqrt{\frac{1}{6} y_i^2 + \frac{1}{3} v_0 f(x_i) \frac{1}{S^2}}. \quad (4.20)$$

2. We then proceed to solve the system of equations by taking adequately small time steps T in the appropriate range $T \in [T_i = 0, T_f]$. We then plot N vs T as given in figure 6 for Starobinsky potential. Typically, N grows linearly with T during near exponential inflation and a substantial decrease in the rate of growth of N indicates the end of inflation.
3. In order to concretely determine the value of N_T , we plot ϵ_H vs N , and note the value of N after which $\epsilon_H \geq 1$. By definition, initially $N = 0$. If $N_T < 70$, then we repeat

⁷Note that for phase-space analysis, we need to incorporate arbitrary values of x_i, y_i (consistent with fixed initial z_i) which may be away from the slow-roll trajectory as discuss below.

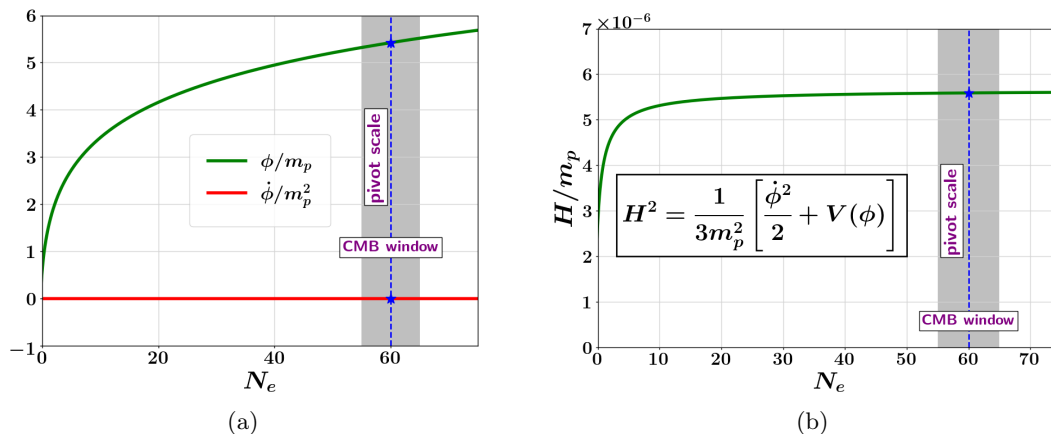


Figure 7: This figure describes the evolution of inflaton field ϕ , and its speed $\dot{\phi}$ in the **left panel**, while the Hubble parameter H in the **right panel** as a function of the number of e-folds before the end of inflation N_e for Starobinsky potential (3.48). Note that during slow-roll inflation, $\dot{\phi}$ and H are nearly constant, while ϕ changes quite slowly. However, ϕ and H begin to change rapidly towards the end of inflation. After inflation ends, ϕ and $\dot{\phi}$ start oscillating around the minimum of the potential (which is not shown in this figure).

this step by increasing the value of x_i , until we get $N_T \geq 70$. (Alternatively, if inflation has not ended⁸, *i.e.* $\epsilon_H < 1$, at the end of our simulation, then either one can increase the value of T_f or decrease x_i . We suggest the latter.) We can then define the number of e-folds before the end of inflation to be $N_e = N_T - N$.

4. The pivot scale can then be fixed to an appropriate value, for example $N_e = 60$, as used in this work. Figure 7 describes the evolution of ϕ , $\dot{\phi}$, and H , while figure 8 illustrates the dynamics of slow-roll parameters ϵ_H , $|\eta_H|$ for Starobinsky potential, as determined from our code. As mentioned before, we usually plot the dynamics of inflation as a function of N_e .
5. In order to accurately fix the value of v_0 , we need to impose $A_S = 2.1 \times 10^{-9}$ at the pivot scale $N_e = 60$. If A_S is lower than expected for the given value of v_0 , then we increase the value of v_0 or vice versa until we arrive at the correct value of A_S , and fix the corresponding value of v_0 .

Following the aforementioned algorithm, we can easily simulate the inflationary background dynamics and investigate the evolution of relevant quantities of our interest. Before going forward, we would like to stress that many of the aforementioned steps (in the present version of our code) are rather meant to be carried out manually by the user. While we are already developing an automated version of this code (which will be presented in the revised version of our paper), we believe that the present version will help the user to understand the inflationary dynamics much better.

⁸Note that if one simulates the cosmological equations in terms of number of e-folds N , rather than cosmic time t , this step can usually be avoided by simulating the system from $N = 0$ to $N = 70$. However, one has to adjust the value of x_i in order to get enough inflation.

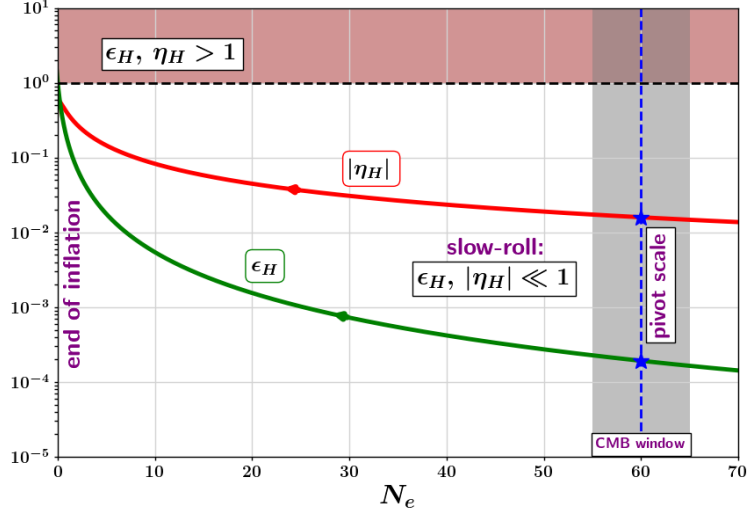


Figure 8: Evolution of the slow-roll parameters ϵ_H and η_H is shown as a function of the number of e-folds before the end of inflation N_e for Starobinsky potential (3.48). From this plot, it is easy to notice that at early times when $N_e \gg 1$, the slow-roll conditions are satisfied *i.e.* $\epsilon_H, |\eta_H| \ll 1$. However, the slow-roll conditions are violated towards the end of inflation (marked by $N_e = 0$ and $\epsilon_H = 1$).

4.1 Phase-space analysis

Phase-space analysis of inflationary dynamics is usually carried out to determine the set of initial conditions that results in adequate amount of inflation, and hence it is important to access the generality of initial conditions for inflation [20, 50, 69]. For a spatially flat background, the phase-space portrait consists of trajectories of $\{\phi, \dot{\phi}\}$ for different initial conditions, with fixed H_i . The standard algorithm to generate such a plot is the following.

1. The initial energy scale of inflation is kept constant by fixing the value of initial Hubble parameter in the phase-space portrait simulations. A typical value often used is $H_i \leq m_p$ (see [20] for detail). Hence, the user is expected to incorporate an appropriate value of z_i .
2. One can then input a suitable value of x_i and determine the value of y_i for a given potential function $f(x)$ from the dimensionless Friedmann equation (4.20) as

$$y_i = \pm \sqrt{6} \sqrt{z_i^2 - \frac{1}{3} v_0 f(x_i) \frac{1}{S^2}}. \quad (4.21)$$

3. With these initial conditions, one can then simulate the system of dimensionless differential equations for $\{x, y, z, A\}$ from $T_i = 0$ till an appropriate T_f . One can then repeat the same step by incorporating a number of different values of x_i in order to generate the phase-space portrait for the given potential. We provide the GitHub link to our phase-space portrait framework [here](https://github.com/bhattsidharth/NumDynInflation/blob/main/inf_dyn_phase.py)⁹. The phase-space portraits for Starobin-

⁹https://github.com/bhattsidharth/NumDynInflation/blob/main/inf_dyn_phase.py

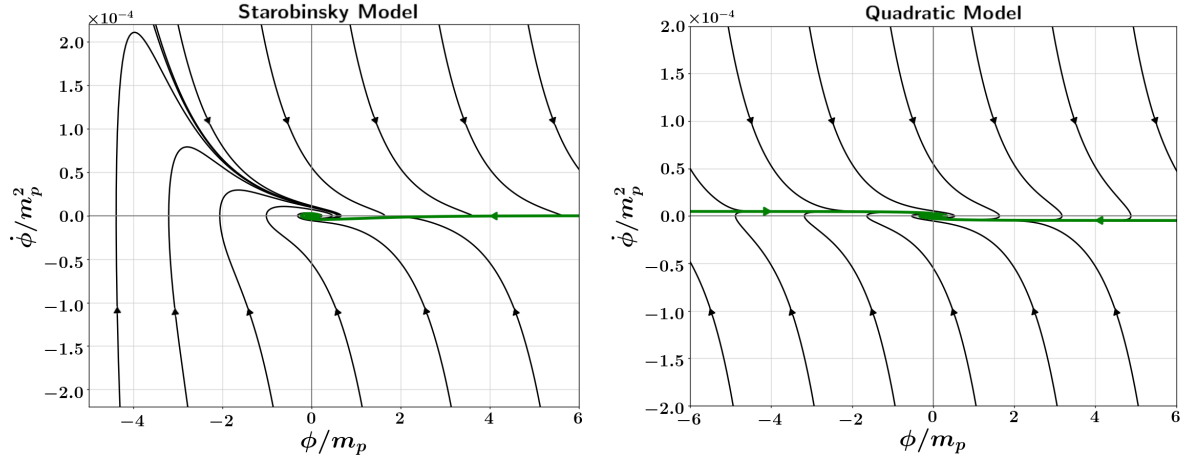


Figure 9: The phase-space portrait $\{\phi, \dot{\phi}\}$ of the inflaton field has been illustrated for Starobinsky potential (3.48) in the **left panel**, and for quadratic potential $V(\phi) = \frac{1}{2} m^2 \phi^2$ in the **right panel** corresponding to different initial conditions $\{\phi_i, \dot{\phi}_i\}$ (plotted in solid black colour) with a fixed initial scale H_i . The figure demonstrates that trajectories commencing from a large class of initial field values (including those with large initial velocities $\dot{\phi}_i$) quickly converge towards the slow-roll attractor separatrix $\dot{\phi} = -V_{,\phi}/3H \simeq \text{const.}$ (plotted in green colour) as can be seen from the rapid decline in the inflaton speed until they meet the green colour curve. After the end of inflation, the inflaton begins to oscillate around the minimum of the potential.

sky potential (3.48), and quadratic potential $V(\phi) \propto \phi^2$ are illustrated in the left and right panels of figure 9 respectively.

In order to determine the degree of generality of inflation, we need to define a measure for the distribution of $\{\phi_i, \dot{\phi}_i\}$. The correct choice for the measure might depend on the quantum theory of gravity. However, a uniform measure is usually considered in the literature. Interested readers are referred to [20, 69] for further detail.

4.2 Quantum fluctuations under the slow-roll approximation

In section 3, we described the expressions for a number of inflationary observables such as A_S , A_T , n_S , n_T , and r associated with the scalar and tensor power spectra which can be determined purely from the dynamics of background quantities such as H , ϵ_H , η_H under the slow-roll approximation. Hence they can be conveniently determined from our background dynamics code as discussed earlier in section 4. For example, the scalar and tensor power spectra for Starobinsky inflation have been plotted in figure 10 as a function N_e . Similarly, one can plot the spectral indices¹⁰ $n_S - 1$ and n_T and determine their values at the pivot scale N_* . The spectral indices for Starobinsky potential have been plotted in figure 11.

¹⁰In the standard literature, one usually plots r vs n_S for a given inflaton potential for a range of possible values of $N_* \in [50, 60]$ which can also be done easily using our code.

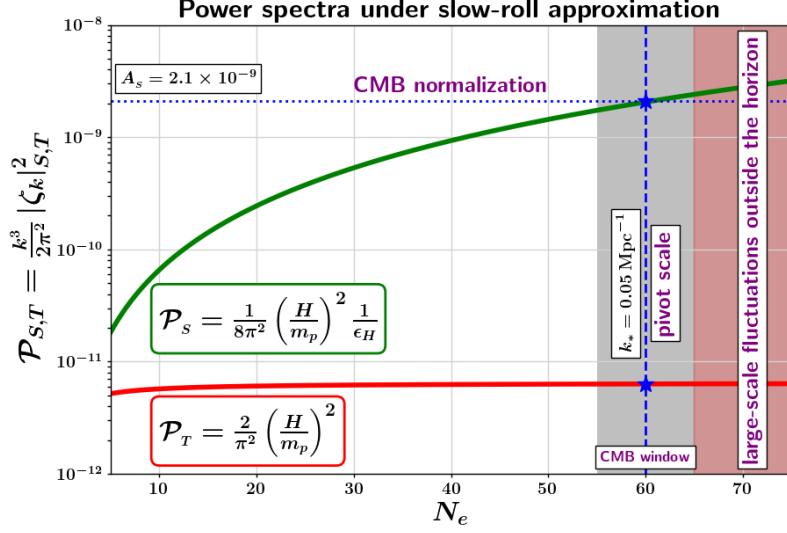


Figure 10: The power spectra of scalar and tensor quantum fluctuations (computed using the slow-roll formulae (3.10) and (3.25) respectively) are shown for comoving modes exiting the Hubble radius at different number of e-folds N_e before the end of inflation for Starobinsky potential (3.48). The CMB window (shown in grey shaded region) corresponds to comoving modes in the range $k_{\text{CMB}} \in [0.0005, 0.5] \text{ Mpc}^{-1}$ that are being probed by the current CMB missions. Fluctuations over larger scales (shown in red shaded region) are outside the observable universe at present and those over smaller scales remain to be (potentially) probed by a plethora of upcoming missions, from GW observatories to PBHs.

5 Numerical analysis for quantum fluctuations during inflation

In the previous section we used slow-roll approximated formulae to study the spectra of inflationary fluctuations in terms of background quantities such as H , ϵ_H , η_H . Hence, we only had to simulate the background dynamics for a given potential in order to plot the relevant inflationary observables. However, if we want to analyze the behaviour of quantum fluctuations more accurately, especially in situations where one or both the slow-roll conditions (2.20) are violated, we need to numerically solve the Mukhanov-Sasaki equation (3.4) corresponding to each comoving scale k .

For this purpose, we first rewrite the Mukhanov-Sasaki equation (3.4) in cosmic time as

$$\frac{d^2 v_k}{dt^2} + H \frac{dv_k}{dt} + \left[\frac{k^2}{a^2} - \frac{1}{a^2} \frac{z''}{z} \right] v_k = 0. \quad (5.1)$$

Note that here z is not the dimensionless Hubble parameter used in our numerical code, rather it is the variable $z = am_p \sqrt{2\epsilon_H}$ in the Mukhanov-Sasaki equation (3.4). The effective mass term z''/z in (3.6) can be re-written as

$$\frac{z''}{z} = a^2 \left[\frac{5}{2} \frac{\dot{\phi}^2}{m_p^2} + 2 \frac{\dot{\phi}\ddot{\phi}}{H m_p^2} + 2H^2 + \frac{1}{2} \frac{\dot{\phi}^4}{H^2 m_p^4} - V_{,\phi\phi}(\phi) \right]. \quad (5.2)$$

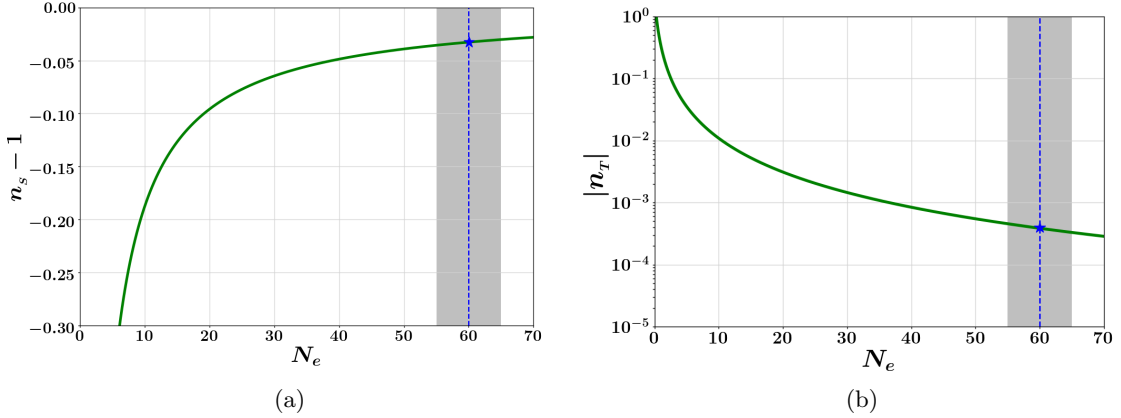


Figure 11: The scalar and tensor spectral indices n_s and n_T are shown as a function of N_e for Starobinsky potential (3.48) as determined by their slow-roll approximated formulae (3.23) and (3.26) respectively. Around the pivot scale, they take the approximate values $n_s \simeq 0.967$ and $n_T \simeq -0.0004$. Note that we have plotted $n_s - 1$ (instead of n_s) since it is the correct scalar spectral index. The tensor-to-scalar ratio is given by $r \simeq -8n_T$.

Since v_k is a complex valued function, it is convenient to split it into its real and imaginary parts to study their evolution separately for the numerical analysis. While both will follow the same evolution equation, they will be supplied with different initial conditions in the form of the real and imaginary parts of the Bunch-Davies vacuum (3.8). Writing the Mukhanov-Sasaki equation for scalar fluctuations in terms of dimensionless variables, we obtain

$$\left[\frac{d^2 v_k}{dT^2} + z \frac{dv_k}{dT} + \left[\frac{k^2}{A^2} - \frac{5}{2} y^2 + 2 \frac{y}{z} \left(3 z y + \frac{v_0}{S^2} f_{,x} \right) - 2 z^2 - \frac{1}{2} \frac{y^4}{z^2} + \frac{v_0}{S^2} f_{,xx} \right] v_k = 0 \right]. \quad (5.3)$$

Our primary goal in this section is to numerically solve equation (5.3) for the Fourier modes v_k corresponding to each comoving scale k and plot the frozen value of the scalar power spectrum of ζ_k given by (3.9) after the mode becomes super-Hubble. We can conveniently relate a comoving scale k to its Hubble-exit epoch by $k = aH$. Since we are only interested in the super-Hubble power spectra, we only need to simulate the system to evolve v_k for a small duration of time around the Hubble-exit of scale k (which should be sufficiently early enough to impose Bunch-Davies initial conditions and sufficiently late enough for the mode to be frozen outside the Hubble radius).

In the following, we discuss the algorithm to solve the Mukhanov-Sasaki equation (5.3) and determine the scalar power spectrum (3.9) numerically. We also discuss how to solve the corresponding equation (3.18) for the tensor power spectrum (at linear order in perturbation theory)¹¹. The dimensionless Mukhanov-Sasaki equation for tensor fluctuations is given by

¹¹Second-order tensor fluctuations which are induced by first-order scalar fluctuations will be discussed in the revised version of our manuscript.

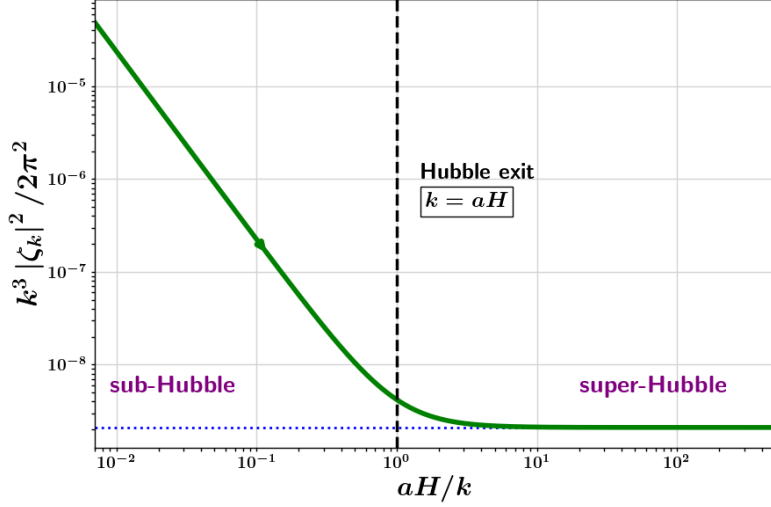


Figure 12: Evolution of scalar power $\frac{k^3}{2\pi^2}|\zeta_k|^2$ is plotted by numerically solving the Mukhanov-Sasaki equation (5.3) for a mode exiting the Hubble radius at about 60 e-folds before the end of inflation (for Starobinsky potential). At early times when the mode is sub-Hubble, *i.e.* $k \gg aH$, the power decreases as $\mathcal{P}_\zeta \sim (aH)^{-2}$ as expected. After the Hubble-exit, the power freezes to a constant in the super-Hubble regime when $k \ll aH$. We note down its value after the mode-freezing as the super-Hubble scale power corresponding to that mode. Repeating the procedure for a range of scales k yields us the power spectrum of scalar fluctuations. The same numerical analysis can be carried out for tensor fluctuations.

$$\left[\frac{d^2 h_k}{dT^2} + z \frac{dh_k}{dT} + \left[\frac{k^2}{A^2} + \frac{1}{2} y^2 - 2 z^2 \right] h_k = 0 \right]. \quad (5.4)$$

We explicitly write down the Mukhanov-Sasaki equations for scalar and tensor fluctuations in terms of dimensionless variables (as used in our code) in the following way

$$v_{k,T} = \frac{dv_k}{dT}, \quad (5.5)$$

$$\frac{dv_{k,T}}{dT} = -z v_{k,T} - \left[\frac{k^2}{A^2} - \frac{5}{2} y^2 + 2 \frac{y}{z} \left(3 z y + \frac{v_0}{S^2} f_{,x} \right) - 2 z^2 - \frac{1}{2} \frac{y^4}{z^2} + \frac{v_0}{S^2} f_{,xx} \right] v_k; \quad (5.6)$$

$$h_{k,T} = \frac{dh_k}{dT}, \quad (5.7)$$

$$\frac{dh_{k,T}}{dT} = -z h_{k,T} - \left(\frac{k^2}{A^2} + \frac{1}{2} y^2 - 2 z^2 \right) h_k. \quad (5.8)$$

In our numerical set up, we split v_k and h_k into their real and imaginary parts and simulate them separately with appropriate Bunch-Davies initial conditions. We begin with a discussion of numerical simulations of the Mukhanov-Sasaki equations (5.3) and (5.4) for a purely slow-roll potential (which we choose to be the Starobinsky potential (3.48) as usual),

before moving forward to discuss the same for a potential with a slow-roll violating feature. This latter case is of the primary focus of our paper. In particular, we will illustrate our numerical scheme for the case of a base slow-roll potential possessing a tiny local bump feature, which was proposed in [44] in the context of PBH formation.

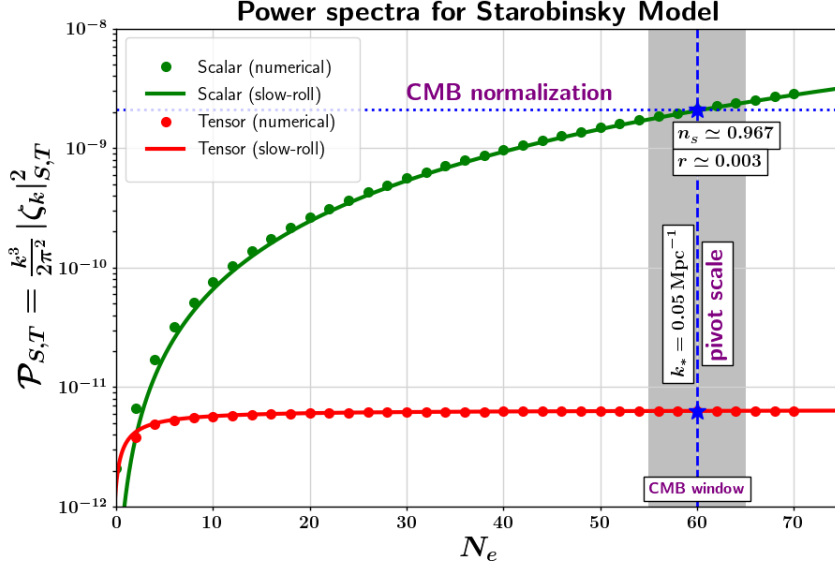


Figure 13: The super-Hubble power spectra of scalar fluctuations (in green colour) and tensor fluctuations (in red colour) are plotted for modes exiting the Hubble radius at different number of e-folds N_e before the end of inflation for Starobinsky potential (3.48). The solid curves represent power spectra computed under the slow-roll approximation (3.10), while the dotted curves represent the power computed by numerically solving the Mukhanov-Sasaki equation (5.3). We conclude that for Starobinsky model, since slow-roll conditions $\epsilon_H, |\eta_H| \ll 1$ are easily satisfied for most part of inflation, the power spectra computed under the slow-roll approximation match quite well with their numerically determined counterparts.

5.1 Numerical analysis for slow-roll potentials

1. As the first step, we numerically solve the background dynamics for a given potential, determine the values of all relevant parameters of the potential and the evolution of relevant primary dynamical variables $\{x, y, z, A\}$ as well as the derived quantities such as $\{N_e, \epsilon_H, \eta_H\}$ (as discussed in section 4).
2. We then proceed to identify different comoving scales k . This can be done by determining their Hubble-exit epochs in the following way. For example, we plot aH (in log scale) against N_e and identify the value of aH at $N_e = N_*$ to be the CMB pivot scale k_p . As mentioned before, we take $N_* = 60$ in all our analysis. Similarly, we associate a corresponding value of N_e to each comoving scale k by the value of aH at its Hubble-exit epoch. This step ensures that we have a one-to-one correspondence between k and N_e in our analysis and we can use them interchangeably.

3. We intend to impose Bunch-Davies initial conditions for a given mode v_k at an epoch when it is sub-Hubble. As it turns out, for most potentials, the Bunch-Davies initial conditions can be safely imposed as long as $k \geq 100 aH$. Hence, rather than simulating the Mukhanov-Sasaki equation for each mode (making Hubble-exit at the corresponding value of N_e) all through the inflationary history (starting from $\phi_i > \phi_*$), we actually impose the initial conditions from the background solutions for $\{x, y, z, A\}$ at around 5 e-folds before the Hubble-exit of that mode. This step greatly reduces the running-time of the code. We then incorporate the initial value of scale factor A_i at the same epoch, namely $A_i \exp(N_T - N_e - 5)$ and do the same for the initial values of the field x_i , and its derivative y_i . The initial conditions for the mode functions v_k and their derivatives \dot{v}_k can then be safely taken to be of Bunch-Davies type.
4. We solve the set of cosmological equations with these initial conditions for a period of time $T = T_i \rightarrow T = T_f$ such that the mode becomes super-Hubble and its power ($k^3 |\zeta_k|^2 / 2\pi^2$) is frozen to a constant value (see figure 12), which is typically within 5 e-folds after Hubble-exit in the kind of models we are interested in. We note down this frozen value as the value of the power spectrum of that mode. While we have been discussing about scalar fluctuations mostly, the same can be done for tensor fluctuations which we have incorporated in our code.
5. We then select another mode that leaves the Hubble radius at some epoch N_e and repeat the procedure until we have collected the frozen super-Hubble power spectra of a range of scales that we are interested in (see figure 13).

From the above numerical analysis of featureless vanilla potentials which exhibit slow-roll dynamics until close to the end of inflation, we observe that the power spectra of scalar and tensor fluctuations are nearly scale-invariant (with small red-tilt) and their behaviour (as obtained from numerically solving the Mukhanov-Sasaki equation) matches quite well with the analytical predictions under the slow-roll approximations (see figure 13).

However, for potentials exhibiting a small-scale feature at intermediate field values $\phi < \phi_*$, there might exist a short period of slow-roll violating phase before the end of inflation during which slow-roll approximations break down. In particular, as we will see, while the first slow-roll parameter remains small $\epsilon_H \ll 1$, the second slow-roll parameter might become $\eta_H \sim \mathcal{O}(1)$. Hence, a numerical analysis of the Mukhanov-Sasaki equation is desired in order to determine the scalar power spectrum more accurately. This will be the main focus of discussion in the next subsection.

5.2 Numerical analysis for potentials with a local bump/dip feature

In order to facilitate PBH formation, we need a large amplification of scalar power spectrum at smaller scales during inflation. This can be achieved by introducing a small-scale feature in the potential which leads to a transient period of slow-roll violating phase (including a short almost-USR phase). Adequate amplification in the super-Hubble scalar power spectrum results in a large density contrast in the post-inflationary universe (upon the Hubble-entry of the corresponding modes) which in turn can collapse to form PBHs. Usually, such a PBH feature in the potential leads to an increase in the value of the second slow-roll parameter η_H from near-zero to a positive value of $\eta_H \sim \mathcal{O}(1)$.

A number of models with different types of features have been proposed in the recent literature (as mentioned before) that facilitate the amplification of scalar power spectrum at

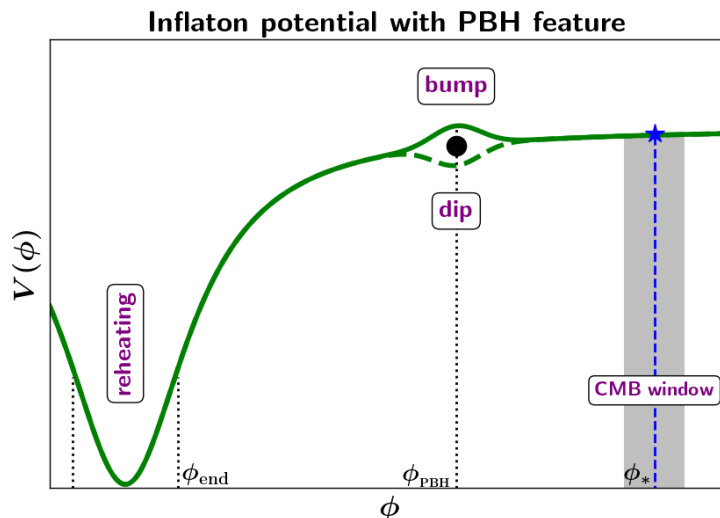


Figure 14: This is a schematic plot of an asymptotically-flat inflationary potential with a tiny bump/dip feature (5.9) near intermediate field values $\phi \simeq \phi_{\text{PBH}}$ that leads to an enhancement of the scalar power spectrum. The full potential asymptotes to the base (slow-roll) potential near the CMB window $\phi \simeq \phi_*$, thus satisfying observational constraints on large cosmological scales. Slow-roll is violated around the feature, whose position ϕ_{PBH} dictates the range of moving scales k that receive amplification of power (which accordingly determines the mass and abundance of formed PBHs). Note that the feature has been greatly exaggerated for illustration purpose. In most realistic models, both the height and the width of the feature are too small to be seen (without zooming-in considerably).

small scales. The most common amongst them is an inflection point-like feature. However, we choose the model proposed in [44] in which the base inflaton potential $V_b(\phi)$ possesses a tiny local bump or dip $\pm\epsilon(\phi, \phi_0)$ at an intermediate field value ϕ_0 of the form

$$V(\phi) = V_b(\phi) [1 \pm \epsilon(\phi, \phi_0)] , \quad (5.9)$$

where we assume $V_b(\phi)$ to be a symmetric or an anti-symmetric asymptotically-flat potential in order to satisfy CMB constraints at large cosmological scales. Such a potential has been schematically illustrated in figure 14. To be specific, in this paper we choose the base potential to be the D-brane KKLT potential [70–73] with a tiny Gaussian bump of the form [44]

$$V(\phi) = V_0 \frac{\phi^2}{m^2 + \phi^2} \left[1 + A \exp \left(-\frac{1}{2} \frac{(\phi - \phi_0)^2}{\sigma^2} \right) \right] , \quad (5.10)$$

where m is a mass scale in the KKLT model, while A and σ represent the height and the width of the tiny bump respectively. We use this particular model to demonstrate our numerical framework because of its simplicity and efficiency. However, one can choose any model of their interest. Values of all the parameters appearing in (5.10), which we use in our numerical analysis, have been explicitly shown in figure 17.

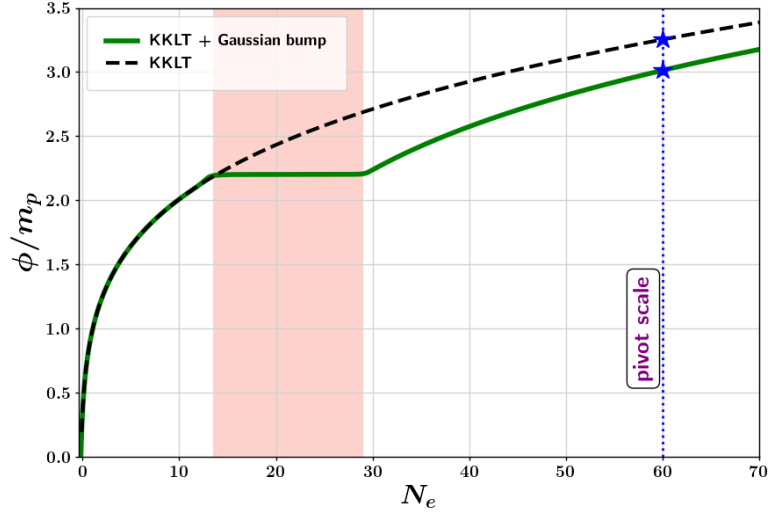


Figure 15: Evolution of the field value ϕ for the KKLT potential with a tiny bump (5.10) is shown in solid green curve as a function of number of e-folds N_e before the end of inflation. We note that at CMB scales, ϕ is much smaller than the corresponding value in the base model (KKLT) (shown in dashed black curve). At intermediate scales when the inflaton evolves across the bump feature in the potential, we gain a lot of extra e-folds of expansion $\Delta N_e \simeq 15$ with little change in the field value. After crossing the feature, evolution of ϕ mimics its corresponding value in the base model.

The height and the width of the (bump/dip) feature required to facilitate adequate amount of power amplification are quite small, and hence the feature is tiny and local (in contrast to inflection point-like features). This ensures that the feature does not significantly affect the CMB observables. However, since we gain a lot of extra e-folds of expansion $\Delta N_e \simeq 15$ with little change in the field value (as shown in figure 15) when the inflaton crosses the feature, the CMB pivot scale gets shifted towards smaller values as compared to the same for the base potential.

Since slow-roll is violated in these models (as shown in figure 16), we need to solve the Mukhanov-Sasaki equation numerically in order to accurately compute the scalar power spectrum. This has been explicitly demonstrated in figure 17. Note that the inflationary dynamics in such models contains a number of phases that include an early slow-roll phase **SR-I** near the CMB window, a transition **T-I** from the early **SR-I** to the subsequent almost ultra slow-roll phase **USR** and a transition **T-II** back to the next slow-roll phase **SR-II** after passing through an intermediate constant-roll phase **CR** (shown in figure 16).

The effective mass term z''/z in the Mukhanov-Sasaki equation (3.4), which primarily governs the dynamics of scalar fluctuations, has been shown in figure 18, and the resultant Hubble-exit behaviour of different modes is described in figure 19. As the inflaton approaches the PBH feature, η_H starts to increase rapidly. This is accompanied by an initial sharp dip in the effective mass term z''/z , which then increases to a higher plateau as η_H approaches its maximum in the USR type phase. The modes that leave the Hubble radius slightly before the transition already start receiving power amplification on super-Hubble scales as shown

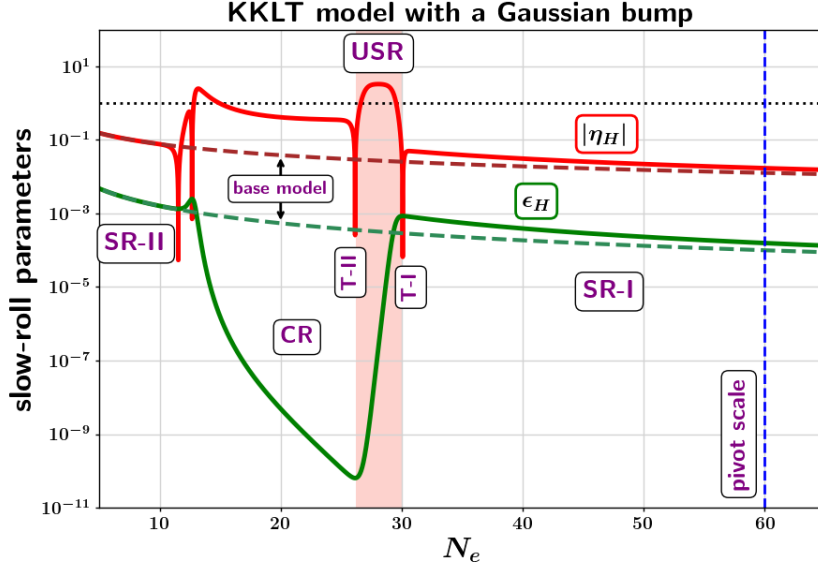


Figure 16: Evolution of the slow-roll parameters ϵ_H and η_H is shown in solid green and solid red curves respectively for the KKLT potential with a tiny bump (5.10). Both ϵ_H and η_H are close to their corresponding values for the base KKLT potential (shown in dashed curves) at early times near the CMB window. At $N_e \simeq 30$, the value of ϵ_H starts decreasing rapidly leading to an increase in η_H from $|\eta_H| \ll 1$ to a higher and positive value $\eta_H \simeq +3.3$ (almost USR phase). Thereafter, the inflaton enters a phase of constant-roll inflation (where $\eta_H \simeq -0.37$) before returning to the final slow-roll phase.

by the orange color curve in figure 19.

It is worth noting that the power spectrum exhibits a dip which corresponds to very narrow range of scales $k \simeq k_{\text{dip}}$ that leave the Hubble radius a few e-folds before the USR phase (shown by the blue color curve in figure 19). The maximum rate of growth observed in this model is consistent with the steepest growth bound discussed in [65]. Near the USR phase when $\eta_H \gtrsim 3$, z''/z saturates to a constant value. Modes leaving the Hubble radius around this USR epoch receive maximal amplification in their super-Hubble power spectrum.

As the field crosses the maximum of the bump feature, η_H decreases to a constant negative value. It stays in this constant-roll phase until the inflaton meets the base potential eventually and approaches the final slow-roll phase in its dynamics before the end of inflation. The dynamics of scalar fluctuations in the aforementioned phases are quite rich, and interesting. However, since the main aim of this paper is to illustrate how to use our numerical code with an example, we do not discuss these phases and their impact on the power spectrum (some of which have been explicitly shown in figures 18, 19, 20), and refer the interested readers to [63] for more detail.

6 Future extension of our numerical framework

In preceding sections, we described the relevant cosmological equations governing the inflationary dynamics in terms of dimensionless variables. We also introduced our numerical code

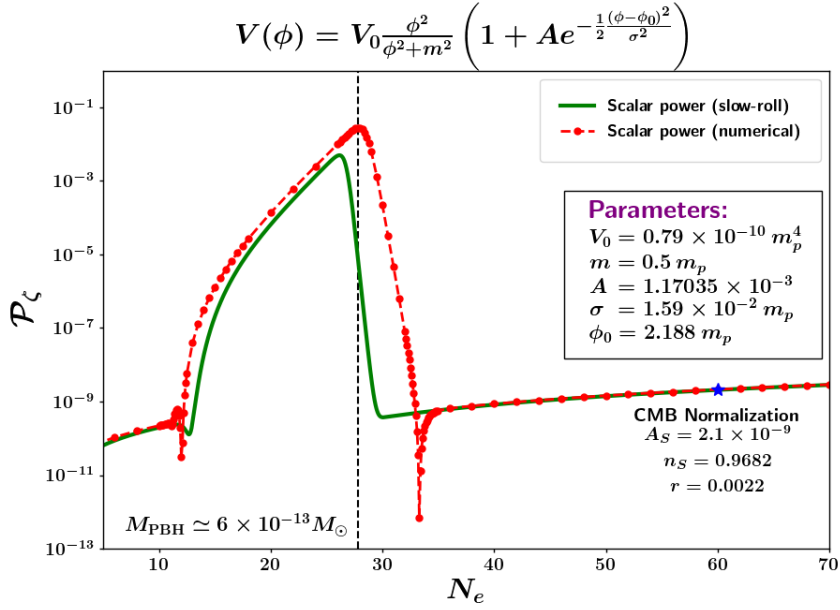


Figure 17: The super-Hubble power spectra of scalar fluctuations are plotted for modes exiting the Hubble radius at different number of e-folds N_e before the end of inflation for KKLT potential with a tiny bump (5.10). The solid green curve represents the power spectrum computed under the slow-roll approximation (3.10), while the dotted red curve represents the power computed by numerically solving the Mukhanov-Sasaki equation (5.3). Since the second slow-roll condition is violated due to the presence of the bump (leading to $\eta_H > 1$), the slow-roll approximation underestimates the value of power spectrum near the peak (as well as the position of the peak) for modes exiting the Hubble radius near the epoch when the inflaton crosses the local maximum around the bump feature. This leads to an incorrect estimation of the mass fraction as well as the central mass of the PBHs formed in this scenario.

(written in terms of cosmic time) that can easily simulate the inflationary dynamics both at the background level in section 4 and at linear order in perturbation theory in section 5. However, with minimal to moderate extension, our numerical code can be used to simulate a number of different scenarios associated with scalar field dynamics both during inflation as well as in the post-inflationary universe. We have already started working on some of these aspects which will appear in the revised version of our manuscript. In the following we discuss some of the important future extensions of our code that we intend to include in our revised version.

1. As stressed in section 4, the present version of our numerical code, although quite fast and neat, contains segments that require the user to carry out a number of tasks manually. While we believe that the present version will definitely help a user (who is relatively new to the field) to understand the inflationary dynamics much better, we are already developing an automated version of this code that is much more compact and requires substantially less manual involvement of the user. We also plan to make the code even faster. We will present the updated version of our code in the revised

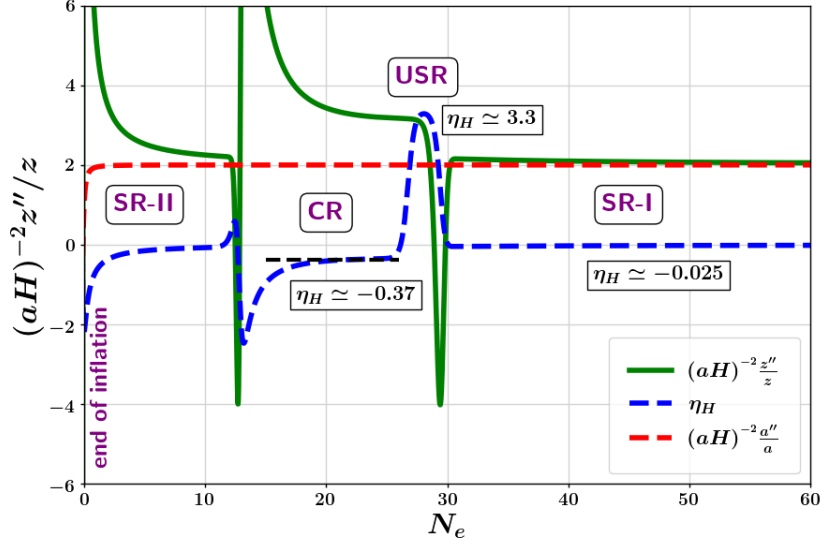


Figure 18: Evolution of the effective mass term in the Mukhanov-Sasaki equation is shown here in solid green curve for the KKLT potential with a tiny bump (5.10). Important transient phases of the scalar field dynamics are also highlighted following the behaviour of the second slow-roll parameter η_H (plotted in dashed blue curve). There is a sharp dip in the effective mass term when the field transitions from the first slow-roll phase (SR-I) to an almost ultra slow-roll phase (USR). The inflaton later makes a transition to a phase of constant-roll inflation with $\eta_H \simeq -0.37$, before reaching a final slow-roll phase until the end of inflation.

version of our paper and refer to it in the same [GitHub link](#) ¹².

2. In section 5, we briefly discussed how to solve the evolution equation for the tensor fluctuations at linear order in perturbation theory. However, first-order scalar fluctuations induce tensor fluctuations at second order in perturbation theory which might be significant when slow-roll is violated, especially in the scenario where scalar power spectrum is largely amplified in order to source PBH formation. We will incorporate the computation of such scalar-induced Gravitational Waves in the updated version of our code.
3. In our analysis, we used the Mukhanov-Sasaki variable v_k with its corresponding evolution equation (5.1) in order to simulate scalar fluctuations at linear order. Our code runs quite quickly and generates the power spectrum without requiring a large computational time. However, one can study the scalar power spectrum by using other variables proposed in the literature. We are particularly interested in two such variables. The first one is the curvature perturbation ζ_k itself using the corresponding evolution equation (3.11). For example, it was claimed in [74] that numerical simulations are more stable in terms of ζ_k since it is explicitly frozen well outside the Hubble radius. Similarly, authors of [75] have suggested a change in the variable v_k in the

¹²<https://github.com/bhattsidharth/NumDynInflation>

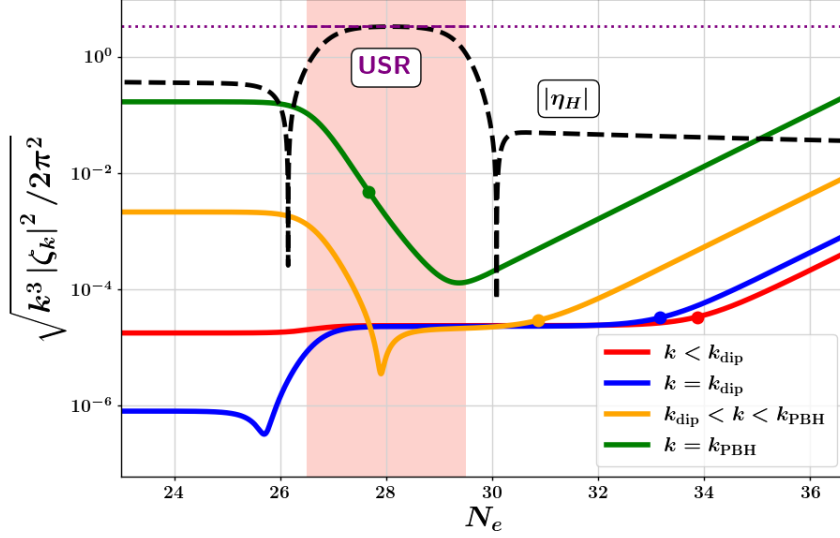


Figure 19: This figure demonstrates the horizon exit behaviour of different modes *i.e* the evolution of $\sqrt{\mathcal{P}_\zeta}$ for different modes as they cross the Hubble radius in KKLT model with a Gaussian bump (5.10). The dot on each curve corresponds to its Hubble-exit epoch. The sharp dip in the power spectrum (figure 17) corresponds to the mode k_{dip} (plotted in blue color) that exits the Hubble radius a few e-folds before the commencement of the USR phase. The mode k_{PBH} which exits the Hubble radius during the USR phase receives a maximal amplification of power (plotted in green color).

form $g_k \equiv \frac{v_k}{z} e^{ik\tau}$ that is supposed to make the simulations much more stable since it removes the early time oscillations¹³.

In the revised version of our work, we plan on carrying out a comprehensive numerical analysis to compare both stability as well speed of the numerical simulations using all three of the aforementioned variables v_k , ζ_k , and g_k .

4. It is easy to extend our numerical analysis to incorporate the dynamics of more than one scalar fields during inflation, at least in the background level. In the future, we are going to provide an updated numerical code to study both the background dynamics as well as quantum fluctuations in two-field inflationary dynamics (where the second field might also source inflation, or act as a spectator field).
5. Additionally, our code can be extended to simulate the post-inflationary dynamics of the inflaton field as well as to study parametric resonance by simulating the evolution of different Fourier modes of the inflaton fluctuations. During the post-inflationary oscillations, it is usually advisable to make a change in the Mukhanov-Sasaki variable of the form $\tilde{v}_k = a^{1/2} v_k$ as suggested in [76, 77]. The code can also be extended to study the dynamics of scalar field dark matter and quintessence by suitably redefining the dimensionless variables as per the energy scale of the dynamics.

¹³We are thankful to Christian Byrnes for bringing this to our attention.

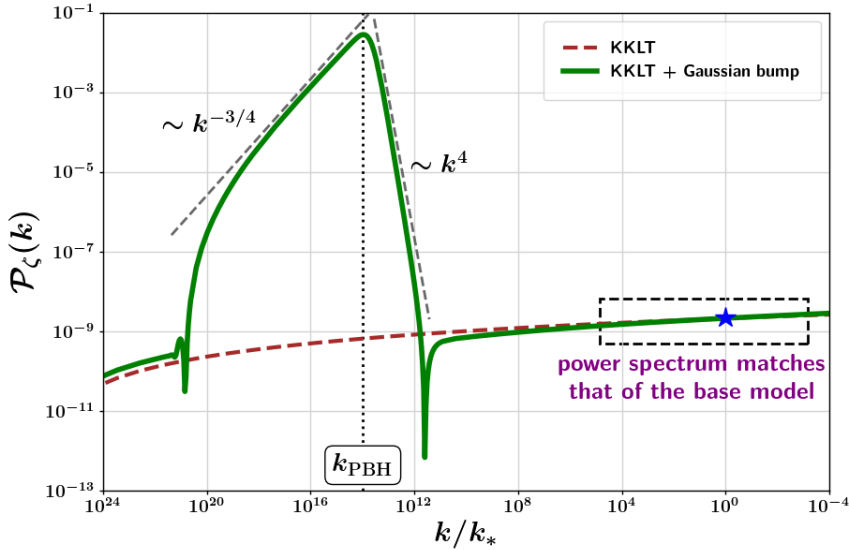


Figure 20: The super-Hubble power spectrum of scalar fluctuations obtained by numerically solving the Mukhanov-Sasaki equation (5.3) is plotted here for the KKLT potential with a tiny bump (5.10). At large scales (around the CMB window), the power spectrum matches that of the base KKLT potential. The power spectrum (after exhibiting a sharp dip) receives a large amplification at intermediate scales $k \sim k_{\text{PBH}}$ around the USR phase. The maximum rate of growth observed in this model is consistent with the steepest growth bound discussed in [65]. After reaching the peak, the power then decreases at a steady rate during the constant-roll phase before finally asymptoting towards its base slow-roll value towards the end of inflation.

7 Discussion

In the present version of our manuscript, we introduced our numerical approach to simulate the cosmological equations in order to study the inflationary dynamics at the level of both background as well as linear-order in perturbation theory. We provided the link to our open-source `GitHub` repository where we have supplied a `Python`-based simple numerical code to simulate inflationary dynamics in terms of cosmic time t . We explicitly demonstrated how to use the code to study the inflationary background dynamics in section 4 that includes plotting the phase-space portrait of inflation as well as to characterise quantum fluctuations during inflation using the simulations of the background dynamics.

Section 5 was dedicated to study quantum fluctuations during inflation (without using slow-roll approximated expressions) by numerically solving the mode function equations of scalar and tensor fluctuations. For a featureless slow-roll inflaton potential, the difference between the results obtained numerically and those obtained under slow-roll approximations were negligible until close to the end of inflation, as expected. We used the Starobinsky potential (3.48) as an example to illustrate our analysis. Our primary focus was the numerical evaluation of the scalar power spectrum $\mathcal{P}_\zeta(k)$ for potentials that exhibit a slow-roll violating feature. In particular, we used the example of an asymptotically-flat base inflationary

potential that possesses a tiny local bump feature (5.9) to illustrate our numerical scheme in section 5.2. By suitably choosing the parameters of the potential (5.10), one can achieve a large enough amplification of the scalar power spectrum in order to facilitate the formation of PBHs in the post-inflationary epoch.

In our numerical analysis for the case of potentials with a slow-roll violating feature, we explicitly chose the parameters in order to amplify the small-scale scalar power by a factor of $\sim 10^7$ with respect to the corresponding power at large cosmological scales, as is usually assumed in the literature to facilitate the formation of PBHs in the subsequent radiation dominated epoch. However, it is important to stress that a significant growth in the scalar power spectrum at small-scales might engender the dynamics to enter into non-perturbative regime. For example, a careful computation of loop corrections to the two-point scalar fluctuations demonstrates [78, 79] that contribution from 1-loop effects becomes of the same order as the tree-level computation (which we carried out in this work) if $\mathcal{P}_\zeta(k) \sim 10^{-2}$ indicating a breakdown of the perturbative analysis.

Moreover, the mechanism of PBH formation in the context of single field models of inflation involves additional intricacies that demand for a non-perturbative analysis of primordial fluctuations. Firstly, a sharp drop in the classical drift speed of the inflaton due to the presence of the PBH-producing feature often incites the system to enter into a phase where stochastic quantum diffusion effects become non-negligible, at times even significant. More importantly, since PBHs form from rare extreme peaks, and hence are determined by the tail of the probability distribution function (PDF) $P[\zeta]$ of the primordial fluctuations, perturbative computations based on only power-spectrum lead to an inaccurate estimation of the PBH mass fraction. Consequently, determination of the full primordial PDF becomes crucial, which can be computed non-perturbatively using the stochastic inflation framework [80–105], which usually predicts a non-Gaussian exponential tail [86, 90]. Tail of the primordial PDF can also be computed by using semi-classical techniques discussed in [106]. Determining the tail of the primordial PDF is an important and active topic of research [90, 106–111] at present, which is beyond the scope of our perturbative analysis presented here.

Before concluding, let us mention that we also stressed upon various important future extensions of our numerical scheme in section 6 that will result in making our code more efficient, and enable us to simulate the scalar field dynamics in a number of interesting scenarios. This includes updating our code to make it more compact and automated, as well as extending it to study the spectrum of scalar-induced gravitational waves, inflaton dynamics in the post-inflationary epoch, multi-field inflationary dynamics, and even scalar field models of dark matter and dark energy. We will incorporate most of these additional features in the revised version of our manuscript. In the meantime, we welcome constructive comments and suggestions as well as queries from interested readers which will help us in improving the quality of our numerical work and presentation in the updated version of the paper.

8 Acknowledgements

S.S.M thanks Satadru Bag, Shabbir Shaikh, and Varun Sahni for crucial inputs during the early stages of development of this code. The authors are grateful to Parth Bhargava and Sanket Dave for stimulating discussions on various topics related to numerical dynamics discussed in this paper. S.S.M. is supported as a postdoctoral Research Associate at the

School of Physics and Astronomy, University of Nottingham by the STFC funded consolidated grant, UK. S.S.B was supported by the INSPIRE scholarship of the Department of Science and Technology (DST), Govt. of India during his Master's thesis work during which a significant portion of this work was carried out.

References

- [1] A. A. Starobinsky, "A New Type of Isotropic Cosmological Models Without Singularity," Phys. Lett. B **91**, 99-102 (1980).
- [2] A. H. Guth, "The Inflationary Universe: A Possible Solution to the Horizon and Flatness Problems," Phys. Rev. D **23**, 347 (1981).
- [3] A. D. Linde, "A New Inflationary Universe Scenario: A Possible Solution of the Horizon, Flatness, Homogeneity, Isotropy and Primordial Monopole Problems", Phys. Lett. B **108**, 389 (1982).
- [4] A. Albrecht and P. J. Steinhardt, "Cosmology for Grand Unified Theories with Radiatively Induced Symmetry Breaking," Phys. Rev. Lett. **48**, 1220 (1982).
- [5] A. D. Linde, "Chaotic Inflation," Phys. Lett. B **129**, 177-181 (1983).
- [6] A.D. Linde, *Particle Physics and Inflationary Cosmology*, Harwood, Chur, Switzerland (1990).
- [7] D. Baumann, "TASI Lectures on Inflation", [arXiv:0907.5424].
- [8] V. F. Mukhanov and G. V. Chibisov, JETP Lett. **33**, 532 (1981).
- [9] S. W. Hawking, Phys. Lett. B **115**, 295 (1982).
- [10] A. A. Starobinsky, Phys. Lett. B **117**, 175 (1982).
- [11] A. H. Guth and S. -Y. Pi, Phys. Rev. Lett. **49**, 1110 (1982).
- [12] A.A. Starobinsky, JETP Lett., 30 , 682 (1979).
- [13] V. Sahni, Phys. Rev. D **42**, 453 (1990).
- [14] M. Tegmark, "What does inflation really predict?," JCAP **04** (2005), 001 [arXiv:astro-ph/0410281 [astro-ph]].
- [15] Y. Akrami *et al.* [Planck], "Planck 2018 results. X. Constraints on inflation" Astron. Astrophys. **641**, A10 (2020) [arXiv:1807.06211 [astro-ph.CO]].
- [16] S. S. Mishra, V. Sahni and A. A. Starobinsky, "Curing inflationary degeneracies using reheating predictions and relic gravitational waves," JCAP **05**, 075 (2021) [arXiv:2101.00271 [gr-qc]].
- [17] P. A. R. Ade *et al.* [BICEP and Keck], "Improved Constraints on Primordial Gravitational Waves using Planck, WMAP, and BICEP/Keck Observations through the 2018 Observing Season," Phys. Rev. Lett. **127**, no.15, 151301 (2021) [arXiv:2110.00483 [astro-ph.CO]].
- [18] S. S. Mishra and V. Sahni, "Canonical and Non-canonical Inflation in the light of the recent BICEP/Keck results," [arXiv:2202.03467 [astro-ph.CO]].
- [19] R. Kallosh and A. Linde, "BICEP/Keck and cosmological attractors," JCAP **12**, no.12, 008 (2021) [arXiv:2110.10902 [astro-ph.CO]].
- [20] S. S. Mishra, V. Sahni and A. V. Toporensky, "Initial conditions for Inflation in an FRW Universe," Phys. Rev. D **98**, no.8, 083538 (2018) [arXiv:1801.04948 [gr-qc]].
- [21] S. Hawking, "Gravitationally collapsed objects of very low mass," Mon. Not. Roy. Astron. Soc. **152** (1971), 75
- [22] B. J. Carr and S. W. Hawking, "Black holes in the early Universe," Mon. Not. Roy. Astron. Soc. **168** (1974), 399-415

- [23] B. J. Carr, “The Primordial black hole mass spectrum,” *Astrophys. J.* **201** (1975), 1-19
- [24] M. Sasaki, T. Suyama, T. Tanaka and S. Yokoyama, “Primordial black holes—perspectives in gravitational wave astronomy,” *Class. Quant. Grav.* **35** (2018) no.6, 063001 [arXiv:1801.05235 [astro-ph.CO]].
- [25] G. F. Chapline, “Cosmological effects of primordial black holes,” *Nature* **253** (1975) no.5489, 251-252
- [26] P. Meszaros, “Primeval black holes and galaxy formation,” *Astron. Astrophys.* **38** (1975), 5-13
- [27] P. Ivanov, P. Naselsky and I. Novikov, “Inflation and primordial black holes as dark matter,” *Phys. Rev. D* **50** (1994), 7173-7178
- [28] B. Carr, F. Kuhnel and M. Sandstad, “Primordial Black Holes as Dark Matter,” *Phys. Rev. D* **94** (2016) no.8, 083504 [arXiv:1607.06077 [astro-ph.CO]].
- [29] A. M. Green and B. J. Kavanagh, “Primordial Black Holes as a dark matter candidate,” *J. Phys. G* **48**, no.4, 043001 (2021) [arXiv:2007.10722 [astro-ph.CO]].
- [30] B. Carr and F. Kuhnel, “Primordial Black Holes as Dark Matter: Recent Developments,” *Ann. Rev. Nucl. Part. Sci.* **70** (2020), 355-394 [arXiv:2006.02838 [astro-ph.CO]].
- [31] E. Bugaev and P. Klimai, “Large curvature perturbations near horizon crossing in single-field inflation models,” *Phys. Rev. D* **78** (2008), 063515 [arXiv:0806.4541 [astro-ph]].
- [32] C. Germani and T. Prokopec, “On primordial black holes from an inflection point,” *Phys. Dark Univ.* **18** (2017), 6-10 [arXiv:1706.04226 [astro-ph.CO]].
- [33] J. M. Ezquiaga, J. Garcia-Bellido and E. Ruiz Morales, “Primordial Black Hole production in Critical Higgs Inflation,” *Phys. Lett. B* **776** (2018), 345-349 doi:10.1016/j.physletb.2017.11.039 [arXiv:1705.04861 [astro-ph.CO]].
- [34] J. Garcia-Bellido and E. Ruiz Morales, “Primordial black holes from single field models of inflation,” *Phys. Dark Univ.* **18** (2017), 47-54 [arXiv:1702.03901 [astro-ph.CO]].
- [35] I. Dalianis, A. Kehagias and G. Tringas, “Primordial black holes from α -attractors,” *JCAP* **01** (2019), 037 [arXiv:1805.09483 [astro-ph.CO]].
- [36] O. Özsoy, S. Parameswaran, G. Tasinato and I. Zavala, “Mechanisms for Primordial Black Hole Production in String Theory,” *JCAP* **07** (2018), 005 [arXiv:1803.07626 [hep-th]].
- [37] M. Cicoli, V. A. Diaz and F. G. Pedro, “Primordial Black Holes from String Inflation,” *JCAP* **06** (2018), 034 [arXiv:1803.02837 [hep-th]].
- [38] M. P. Hertzberg and M. Yamada, “Primordial Black Holes from Polynomial Potentials in Single Field Inflation,” *Phys. Rev. D* **97** (2018) no.8, 083509 [arXiv:1712.09750 [astro-ph.CO]].
- [39] G. Ballesteros and M. Taoso, “Primordial black hole dark matter from single field inflation,” *Phys. Rev. D* **97** (2018) no.2, 023501 [arXiv:1709.05565 [hep-ph]].
- [40] H. Di and Y. Gong, “Primordial black holes and second order gravitational waves from ultra-slow-roll inflation,” *JCAP* **07** (2018), 007 [arXiv:1707.09578 [astro-ph.CO]].
- [41] H. Motohashi, S. Mukohyama and M. Oliosi, “Constant Roll and Primordial Black Holes,” *JCAP* **03** (2020), 002 [arXiv:1910.13235 [gr-qc]].
- [42] R. Mahbub, “Primordial black hole formation in inflationary α -attractor models,” *Phys. Rev. D* **101** (2020) no.2, 023533 [arXiv:1910.10602 [astro-ph.CO]].
- [43] N. Bhaumik and R. K. Jain, “Primordial black holes dark matter from inflection point models of inflation and the effects of reheating,” *JCAP* **01** (2020), 037 [arXiv:1907.04125 [astro-ph.CO]].
- [44] S. S. Mishra and V. Sahni, “*Primordial Black Holes from a tiny bump/dip in the Inflaton potential*,” *JCAP* **04**, 007 (2020) [arXiv:1911.00057 [gr-qc]].

- [45] K. Kefala, G. P. Kodaxis, I. D. Stamou and N. Tetradis, “Features of the inflaton potential and the power spectrum of cosmological perturbations,” *Phys. Rev. D* **104** (2021) no.2, 023506 [arXiv:2010.12483 [astro-ph.CO]].
- [46] H. V. Ragavendra, P. Saha, L. Sriramkumar and J. Silk, “Primordial black holes and secondary gravitational waves from ultraslow roll and punctuated inflation,” *Phys. Rev. D* **103** (2021) no.8, 083510 [arXiv:2008.12202 [astro-ph.CO]].
- [47] O. Özsoy and Z. Lalak, “Primordial black holes as dark matter and gravitational waves from bumpy axion inflation,” *JCAP* **01** (2021), 040 [arXiv:2008.07549 [astro-ph.CO]].
- [48] R. Zheng, J. Shi and T. Qiu, “On Primordial Black Holes and secondary gravitational waves generated from inflation with solo/multi-bumpy potential,” [arXiv:2106.04303 [astro-ph.CO]].
- [49] K. Inomata, E. McDonough and W. Hu, “Primordial black holes arise when the inflaton falls,” *Phys. Rev. D* **104** (2021) no.12, 123553 [arXiv:2104.03972 [astro-ph.CO]].
- [50] R. Brandenberger, “Initial conditions for inflation — A short review,” *Int. J. Mod. Phys. D* **26** (2016) no.01, 1740002 [arXiv:1601.01918 [hep-th]].
- [51] D. Baumann, *PoS TASI* **2017**, 009 (2018) [arXiv:1807.03098 [hep-th]].
- [52] J. M. Maldacena, “Non-Gaussian features of primordial fluctuations in single field inflationary models,” *JHEP* **05**, 013 (2003) [arXiv:astro-ph/0210603 [astro-ph]].
- [53] M. Sasaki, “Large Scale Quantum Fluctuations in the Inflationary Universe,” *Prog. Theor. Phys.* **76**, 1036 (1986).
- [54] V. F. Mukhanov, “Quantum Theory of Gauge Invariant Cosmological Perturbations,” *Sov. Phys. JETP* **67**, 1297 (1988) [*Zh. Eksp. Teor. Fiz.* **94N7**, 1 (1988)].
- [55] H. Motohashi, A. A. Starobinsky and J. Yokoyama, “Inflation with a constant rate of roll,” *JCAP* **1509**, 018 (2015) [arXiv:1411.5021 [astro-ph.CO]].
- [56] T. S. Bunch and P. C. W. Davies, “Quantum Field Theory in de Sitter Space: Renormalization by Point Splitting,” *Proc. Roy. Soc. Lond. A* **360**, 117 (1978).
- [57] S. Matarrese, S. Mollerach and M. Bruni, “Second order perturbations of the Einstein-de Sitter universe,” *Phys. Rev. D* **58** (1998), 043504
- [58] D. Baumann, P. J. Steinhardt, K. Takahashi and K. Ichiki, “Gravitational Wave Spectrum Induced by Primordial Scalar Perturbations,” *Phys. Rev. D* **76** (2007), 084019 [arXiv:hep-th/0703290 [hep-th]].
- [59] N. Bartolo, V. De Luca, G. Franciolini, A. Lewis, M. Peloso and A. Riotto, “Primordial Black Hole Dark Matter: LISA Serendipity,” *Phys. Rev. Lett.* **122** (2019) no.21, 211301 [arXiv:1810.12218 [astro-ph.CO]].
- [60] R. g. Cai, S. Pi and M. Sasaki, “Gravitational Waves Induced by non-Gaussian Scalar Perturbations,” *Phys. Rev. Lett.* **122** (2019) no.20, 201101 [arXiv:1810.11000 [astro-ph.CO]].
- [61] G. Domènech, “Scalar Induced Gravitational Waves Review,” *Universe* **7** (2021) no.11, 398 [arXiv:2109.01398 [gr-qc]].
- [62] B. Whitt, “Fourth Order Gravity as General Relativity Plus Matter,” *Phys. Lett. B* **145** (1984), 176-178
- [63] A. Karam, N. Koivunen, E. Tomberg, V. Vaskonen and H. Veermäe, “Anatomy of single-field inflationary models for primordial black holes,” [arXiv:2205.13540 [astro-ph.CO]].
- [64] H. Motohashi and W. Hu, “Primordial Black Holes and Slow-Roll Violation,” *Phys. Rev. D* **96** (2017) no.6, 063503 doi:10.1103/PhysRevD.96.063503 [arXiv:1706.06784 [astro-ph.CO]].
- [65] C. T. Byrnes, P. S. Cole and S. P. Patil, “Steepest growth of the power spectrum and primordial black holes,” *JCAP* **06**, 028 (2019) [arXiv:1811.11158 [astro-ph.CO]].

- [66] P. Carrilho, K. A. Malik and D. J. Mulryne, “Dissecting the growth of the power spectrum for primordial black holes,” *Phys. Rev. D* **100**, no.10, 103529 (2019) [arXiv:1907.05237 [astro-ph.CO]].
- [67] O. Özsoy and G. Tasinato, “On the slope of the curvature power spectrum in non-attractor inflation,” *JCAP* **04**, 048 (2020) [arXiv:1912.01061 [astro-ph.CO]].
- [68] P. S. Cole, A. D. Gow, C. T. Byrnes and S. P. Patil, “Steepest growth re-examined: repercussions for primordial black hole formation,” [arXiv:2204.07573 [astro-ph.CO]].
- [69] V. A. Belinsky, I. M. Khalatnikov, L. P. Grishchuk and Y. B. Zeldovich, “INFLATIONARY STAGES IN COSMOLOGICAL MODELS WITH A SCALAR FIELD,” *Phys. Lett. B* **155** (1985), 232-236.
- [70] S. Kachru, R. Kallosh, A. D. Linde and S. P. Trivedi, “De Sitter vacua in string theory,” *Phys. Rev. D* **68**, 046005 (2003) [arXiv:hep-th/0301240 [hep-th]].
- [71] S. Kachru, R. Kallosh, A. D. Linde, J. M. Maldacena, L. P. McAllister and S. P. Trivedi, “Towards inflation in string theory,” *JCAP* **0310**, 013 (2003) [hep-th/0308055].
- [72] R. Kallosh and A. Linde, “CMB targets after the latest Planck data release,” *Phys. Rev. D* **100**, no.12, 123523 (2019) [arXiv:1909.04687 [hep-th]].
- [73] J. Martin, C. Ringeval and V. Vennin, “Encyclopædia Inflationaris,” *Phys. Dark Univ.* **5-6** (2014), 75-235 [arXiv:1303.3787 [astro-ph.CO]].
- [74] W. J. Handley, A. N. Lasenby, H. V. Peiris and M. P. Hobson, “Bayesian inflationary reconstructions from Planck 2018 data,” *Phys. Rev. D* **100** (2019) no.10, 103511 [arXiv:1908.00906 [astro-ph.CO]].
- [75] S. Rasanen and E. Tomberg, “Planck scale black hole dark matter from Higgs inflation,” *JCAP* **01** (2019), 038 [arXiv:1810.12608 [astro-ph.CO]].
- [76] F. Finelli and R. H. Brandenberger, “Parametric amplification of gravitational fluctuations during reheating,” *Phys. Rev. Lett.* **82** (1999), 1362-1365 [arXiv:hep-ph/9809490 [hep-ph]].
- [77] K. Jedamzik, M. Lemoine and J. Martin, “Collapse of Small-Scale Density Perturbations during Preheating in Single Field Inflation,” *JCAP* **09** (2010), 034 [arXiv:1002.3039 [astro-ph.CO]].
- [78] K. Inomata, M. Braglia and X. Chen, “Questions on calculation of primordial power spectrum with large spikes: the resonance model case,” [arXiv:2211.02586 [astro-ph.CO]].
- [79] J. Kristiano and J. Yokoyama, “Ruling Out Primordial Black Hole Formation From Single-Field Inflation,” [arXiv:2211.03395 [hep-th]].
- [80] A. A. Starobinsky, “STOCHASTIC DE SITTER (INFLATIONARY) STAGE IN THE EARLY UNIVERSE,” *Lect. Notes Phys.* **246**, 107-126 (1986) doi:10.1007/3-540-16452-9_6
- [81] D. S. Salopek and J. R. Bond, “Stochastic inflation and nonlinear gravity,” *Phys. Rev. D* **43**, 1005-1031 (1991) doi:10.1103/PhysRevD.43.1005
- [82] A. A. Starobinsky and J. Yokoyama, “Equilibrium state of a selfinteracting scalar field in the De Sitter background,” *Phys. Rev. D* **50**, 6357-6368 (1994) [arXiv:astro-ph/9407016 [astro-ph]].
- [83] T. Fujita, M. Kawasaki, Y. Tada and T. Takesako, “A new algorithm for calculating the curvature perturbations in stochastic inflation,” *JCAP* **12**, 036 (2013) [arXiv:1308.4754 [astro-ph.CO]].
- [84] T. Fujita, M. Kawasaki and Y. Tada, “Non-perturbative approach for curvature perturbations in stochastic δN formalism,” *JCAP* **10**, 030 (2014) [arXiv:1405.2187 [astro-ph.CO]].
- [85] V. Vennin and A. A. Starobinsky, *Eur. Phys. J. C* **75**, 413 (2015) [arXiv:1506.04732].
- [86] C. Pattison, V. Vennin, H. Assadullahi and D. Wands, *JCAP* **10**, 046 (2017) [arXiv:1707.00537].

- [87] J. M. Ezquiaga and J. García-Bellido, “Quantum diffusion beyond slow-roll: implications for primordial black-hole production,” *JCAP* **08** (2018), 018 [arXiv:1805.06731 [astro-ph.CO]].
- [88] M. Biagetti, G. Franciolini, A. Kehagias and A. Riotto, “Primordial Black Holes from Inflation and Quantum Diffusion,” *JCAP* **07** (2018), 032 [arXiv:1804.07124 [astro-ph.CO]].
- [89] C. Pattison, V. Vennin, H. Assadullahi and D. Wands, “Stochastic inflation beyond slow roll,” *JCAP* **07**, 031 (2019) [arXiv:1905.06300 [astro-ph.CO]].
- [90] J. M. Ezquiaga, J. García-Bellido and V. Vennin, “The exponential tail of inflationary fluctuations: consequences for primordial black holes,” *JCAP* **03** (2020), 029 [arXiv:1912.05399 [astro-ph.CO]].
- [91] H. Firouzjahi, A. Nassiri-Rad and M. Noorbala, “Stochastic Ultra Slow Roll Inflation,” *JCAP* **01** (2019), 040 [arXiv:1811.02175 [hep-th]].
- [92] V. Vennin, “Cosmological Inflation: Theoretical Aspects and Observational Constraints,” (PhD Thesis) tel-01094199.
- [93] G. Ballesteros, J. Rey, M. Taoso and A. Urbano, “Stochastic inflationary dynamics beyond slow-roll and consequences for primordial black hole formation,” *JCAP* **08** (2020), 043 [arXiv:2006.14597 [astro-ph.CO]].
- [94] K. Ando and V. Vennin, “Power spectrum in stochastic inflation,” *JCAP* **04**, 057 (2021) [arXiv:2012.02031 [astro-ph.CO]].
- [95] A. De and R. Mahbub, “Numerically modeling stochastic inflation in slow-roll and beyond,” *Phys. Rev. D* **102**, no.12, 123509 (2020) [arXiv:2010.12685 [astro-ph.CO]].
- [96] D. G. Figueroa, S. Raatikainen, S. Rasanen and E. Tomberg, “Non-Gaussian Tail of the Curvature Perturbation in Stochastic Ultraslow-Roll Inflation: Implications for Primordial Black Hole Production,” *Phys. Rev. Lett.* **127**, no.10, 101302 (2021) [arXiv:2012.06551 [astro-ph.CO]].
- [97] D. Cruces and C. Germani, *Phys. Rev. D* **105**, no.2, 023533 (2022) [arXiv:2107.12735].
- [98] G. Rigopoulos and A. Wilkins, *JCAP* **12**, no.12, 027 (2021) [arXiv:2107.05317].
- [99] C. Pattison, V. Vennin, D. Wands and H. Assadullahi, “Ultra-slow-roll inflation with quantum diffusion,” *JCAP* **04**, 080 (2021) [arXiv:2101.05741 [astro-ph.CO]].
- [100] E. Tomberg, “A numerical approach to stochastic inflation and primordial black holes,” *J. Phys. Conf. Ser.* **2156**, no.1, 012010 (2021) [arXiv:2110.10684 [astro-ph.CO]].
- [101] D. G. Figueroa, S. Raatikainen, S. Rasanen and E. Tomberg, “Implications of stochastic effects for primordial black hole production in ultra-slow-roll inflation,” [arXiv:2111.07437 [astro-ph.CO]].
- [102] Y. Tada and V. Vennin, “Statistics of coarse-grained cosmological fields in stochastic inflation,” *JCAP* **02**, no.02, 021 (2022) [arXiv:2111.15280 [astro-ph.CO]].
- [103] R. Mahbub and A. De, “Smooth coarse-graining and colored noise dynamics in stochastic inflation,” [arXiv:2204.03859 [astro-ph.CO]].
- [104] N. Ahmadi, M. Noorbala, N. Feyzabadi, F. Eghbalpoor and Z. Ahmadi, “Quantum Diffusion in Sharp Transition to Non-Slow-Roll Phase,” *JCAP* **08** (2022), 078 [arXiv:2207.10578 [gr-qc]].
- [105] J. H. P. Jackson, H. Assadullahi, K. Koyama, V. Vennin and D. Wands, “Numerical simulations of stochastic inflation using importance sampling,” *JCAP* **10** (2022), 067 [arXiv:2206.11234 [astro-ph.CO]].
- [106] M. Celoria, P. Creminelli, G. Tambalo and V. Yingcharoenrat, “Beyond perturbation theory in inflation,” *JCAP* **06**, 051 (2021) doi:10.1088/1475-7516/2021/06/051 [arXiv:2103.09244 [hep-th]].

- [107] S. Hooshangi, M. H. Namjoo and M. Noorbala, “Rare events are nonperturbative: Primordial black holes from heavy-tailed distributions,” *Phys. Lett. B* **834** (2022), 137400 [arXiv:2112.04520 [astro-ph.CO]].
- [108] Y. F. Cai, X. H. Ma, M. Sasaki, D. G. Wang and Z. Zhou, “One small step for an inflaton, one giant leap for inflation: A novel non-Gaussian tail and primordial black holes,” *Phys. Lett. B* **834** (2022), 137461 [arXiv:2112.13836 [astro-ph.CO]].
- [109] J. M. Ezquiaga, J. García-Bellido and V. Vennin, “Could ”El Gordo” be hinting at primordial quantum diffusion?,” [arXiv:2207.06317 [astro-ph.CO]].
- [110] Y. F. Cai, X. H. Ma, M. Sasaki, D. G. Wang and Z. Zhou, “Highly non-Gaussian tails and primordial black holes from single-field inflation,” [arXiv:2207.11910 [astro-ph.CO]].
- [111] A. D. Gow, H. Assadullahi, J. H. P. Jackson, K. Koyama, V. Vennin and D. Wands, “Non-perturbative non-Gaussianity and primordial black holes,” [arXiv:2211.08348 [astro-ph.CO]].